Faraday Discussions
Cite this: *Faraday Discuss.*, 2024, **251**, 9

PAPER

Spiers Memorial Lecture: New directions in molecular scattering

George C. Schatz, [a] Alec M. Wodtke *[bcd] and Xueming Yang [ef]

Received 31st January 2024, Accepted 5th March 2024
DOI: 10.1039/d4fd00015c

The field of molecular scattering is reviewed as it pertains to gas–gas as well as gas–surface chemical reaction dynamics. We emphasize the importance of collaboration of experiment and theory, from which new directions of research are being pursued on increasingly complex problems. We review both experimental and theoretical advances that provide the modern toolbox available to molecular-scattering studies. We distinguish between two classes of work. The first involves simple systems and uses experiment to validate theory so that from the validated theory, one may learn far more than could ever be measured in the laboratory. The second class involves problems of great complexity that would be difficult or impossible to understand without a partnership of experiment and theory. Key topics covered in this review include crossed-beams reactive scattering and scattering at extremely low energies, where quantum effects dominate. They also include scattering from surfaces, reactive scattering and kinetics at surfaces, and scattering work done at liquid surfaces. The review closes with thoughts on future promising directions of research.

1. Setting the scene with a little history

The discovery of quantum mechanics[1,2] marks the historical starting point for the field of chemical dynamics, especially once Born and Oppenheimer conceived of an approximation for molecules involving an effective potential energy function created by the average field of the electrons.[3] Soon, the first potential energy surface (PES) for a chemical reaction was calculated,[4,5] the idea of a reaction's transition state was conceived and the first theory of absolute reaction rates was developed.[6,7] With the emerging capabilities of computation,[8] comparisons of

[a]*Dept of Chemistry, Northwestern University, Evanston, Illinois 60208, USA*
[b]*Institute for Physical Chemistry, Georg August University, Goettingen, Germany*
[c]*Max Planck Institute for Multidisciplinary Natural Sciences, Goettingen, Germany. E-mail: alec.wodtke@mpinat.mpg.de*
[d]*International Center for the Advanced Studies of Energy Conversion, Georg August University, Goettingen, Germany*
[e]*Dalian Institute for Chemical Physics, Chinese Academy of Sciences, Dalian, China*
[f]*Department of Chemistry, College of Science, Southern University of Science and Technology, Shenzhen, China*

experiment and theory became possible, allowing the new theoretical concepts to be put to the test. Initially, experiments relied on molecular spectroscopy,[9–11] made more powerful by the invention of the laser[12–14] and the growing use of laser-induced fluorescence (LIF),[15–22] which provided nascent quantum-state population distributions produced by chemical reactions.[23,24]

But it was molecular scattering that revolutionized the study of chemical dynamics, first during the so-called "alkali age",[25,26] then as a tool to study ion–molecule chemistry,[27,28] and especially with the advent of the universal crossed-molecular-beam method,[29] which led to the 1986 Nobel Prize in Chemistry. Experiments were now able to control reactant incidence energy, achieve single-collision conditions and detect product molecules' recoil velocities. Product flux maps gave clear insights into the qualitative nature of a reactions' transition state, allowing direct detection of steric entrance-channel effects, reaction complex formation and, through control of incidence translational energy, the presence of reaction barriers.

In the words of its inventor and chief protagonist: "The idea of crossed molecular beams experiments is in a sense to 'visualize' the details of a chemical reaction by tracing the trajectories of the reaction products".[30] Achieving a rigorous "visualization" of a reaction required the application and rapid development of theory. The calculation of PESs evolved from empirical and semi-empirical models, to Hartree–Fock theory,[31] and to wavefunction-based methods that include electron–electron correlation, and large basis sets such that nearly exact results are obtained for some reactions. Simulating the atomic motions governed by PESs has also advanced, from classical mechanics,[32,33] to time-independent quantum scattering theory,[34–36] to time-dependent wave-packet motion.[37–39] Classical mechanics remains the workhorse. In parallel, density functional theory (DFT)[40] can often perform a balancing act between useful accuracy and affordability and it is increasingly common to see on-the-fly studies that compute the forces as the trajectory proceeds.[41]

The state of the field in 1987 was described prophetically in the Nobel lecture of Yuan T. Lee, from which we extract one quote, where the laureate made a prediction. "In the near future, *ab initio* calculations of potential energy surfaces and exact scattering calculations on…simple…systems will likely provide more detailed and accurate information…than one could possibly learn in the laboratory".[30] We will show examples below demonstrating that this prediction has indeed been realized and that from those calculations, astonishing insights can be obtained.

But a second prediction is of even greater significance to this review: "the fruitful interplay of theory and experiment will then extend to more complicated systems, making chemistry a more exact science".[30] One of the most important characteristics of the new directions being established in molecular scattering relies on a fruitful collaboration of experiment and theory that is far more valuable than the sum of its parts. In the same sense that two eyes provide stereoscopic vision, these two windows into nature allow fundamental insights to crystallize. This process of collaboration is bidirectional. Of course, pure theory can guide experiment by making predictions of unexpected behavior; more importantly however, where the current gold is to be found is when theory can be applied to understand what the experimentalist has unambiguously observed, but cannot understand.

This cooperation of experiment and theory represents the current state-of-the-art and provides a framework for new directions and for this review. The review is organized as follows. In Sections 2 and 3, we provide an overview of, respectively, theoretical and experimental advances made in recent years that serve as our scientific tool kit for approaching new problems. Major advances have been made since the 1986 Nobel lecture and it is important to understand the current tools we work with, as well as to examine the problems we hope to solve. In Section 4, we present a few examples of simple gas-phase scattering problems where theory is so powerful that experiment is perhaps no longer necessary, and in Section 5, examples of more complex problems where theory and experiment collaborate to make progress. Sections 6 and 7 present examples in beam surface scattering analogous to those in Sections 4 and 5, respectively. Section 8 concludes with a discussion of future perspectives.

2. Advances in theoretical methods

Theory has become a powerful tool for the quantitative description of both gas-phase and gas–surface collisions. A key factor for this has been the development of methods including machine learning (ML), which enable the representation of full (or at least high)-dimensional potential energy surfaces (PESs), including multiple PESs that interact *via* spin–orbit or derivative couplings. These surfaces are often derived from a large number of high-quality electronic structure calculations, and they can include all nuclear degrees of freedom for gas-phase systems with 3–8 atoms. For gas–surface systems, only selected degrees of freedom are included. Dynamics calculations are carried out with quantum-dynamics codes that handle the important degrees of freedom (and provide an approximate treatment of other degrees of freedom), and with classical or quasiclassical trajectories as an important alternative for reactions that are outside the ability of quantum calculations. In the following, we describe the potential surface and dynamic method development, as well as methods for describing nonadiabatic effects for bimolecular reactions and gas–surface reactions, focusing on work published mostly in the last 10 years. A discussion of specific systems is provided later, in Sections 4–7. To restrict the scope, we omit studies that did not consider global PESs, and methods concerned primarily with energy transfer and photodissociation rather than with bimolecular and gas–surface reactions.

2.1. High-dimensional ground-state PESs

2.1.1 Gas phase. As just noted, there has been tremendous progress in developing methods for representing gas-phase PESs based on DFT or *ab initio* calculations. These developments have transformed the field, as previously it was the lack of global surfaces that limited progress in modeling chemical reaction dynamics. The choice of electronic structure method is also an important activity where one wants to describe the level of electron correlation, basis set, spin–orbit and other relativistic effects, and multiple surfaces and their couplings at the highest possible level. The literature on electronic structure methods is very extensive, and impossible to describe here, but we note a few highly cited reviews of commonly used codes that are used to determine reactive surfaces.[42–46] We also

note that there has been progress in adapting algorithms to advanced hardware like parallel computing and the use of graphical processing units as computational engines.[47] As one example of what is currently possible (here for a reaction of great importance that turns out to have challenging characteristics for quantum chemistry studies), a recent article that provides a detailed discussion of convergence issues for coupled-cluster calculations was presented by Sun and Zhang for the F + H_2 reaction.[48] This study also described representing the PES using a neural-network-based method and then using the PES to do quantum reactive-scattering calculations.

Concerning methods for representing potential surfaces, there is a long history of doing this with analytical functions in combination with least-squares fitting to determine parameters in the functions. In recent work, the combination of analytical functions with machine learning to determine parameters has become quite important. One example of this is the permutationally invariant polynomial (PIP) approach, as recently reviewed by Bowman and coworkers.[49–52] These papers describe the development of PIP surfaces *via* monomial symmetrization. Additionally, a machine-learning kernel-based approach involving Gaussian process regression has been combined with PIP to determine parameters. Bowman has also reviewed the use of a two-level potential fitting process, the so-called Δ-machine-learning approach, in which PIP is used to develop a lower-level surface based on a large number of DFT calculations, and then machine learning (a neural net) is used to describe the difference between the lower-level surface and a higher-level surface obtained from coupled-cluster calculations.[53] In another direction with machine-learning potentials, Meuwly has developed surfaces using the reproducing kernel Hilbert space method.[54,55] A broader discussion of machine learning for describing global surfaces and many other properties, including the direct determination of rate coefficients, has been presented by Meuwly.[56] This paper includes a general discussion of the merits of ML and least-squares-based representations. Another powerful approach that can be used to directly determine rate coefficients from potentials is ring-polymer molecular dynamics (RPMD), as recently implemented by Guo and coworkers for the S(^{3}P) + H_2 reaction using potentials that were described using the PIP-NN method.[57] However, for that reaction, intersystem crossing dominates the dynamics below 1000 K, which was not included in the RPMD calculation.

2.1.2 Gas–surface. PESs for describing gas–surface dynamics are generally more complicated to develop than gas-phase potentials, so there has been a range of levels of sophistication in what has been generated. Of course, the simplest (but still difficult) activity is to determine barriers for reactions on surfaces using electronic structure calculations. Typically, this is done with density functional theory, but since there are many choices of functionals and pseudopotentials, benchmark comparisons with experiment are essential and, by the way, rare. Two recent papers where this has been done for reactions on metal surfaces are by Nørskov, Kroes and coworkers.[58,59] In these papers, barrier heights from the Vienna Ab Initio Simulation Package (VASP) were obtained for commonly used functionals for the dissociation of small molecules on surfaces that included Cu, Pt, Ru and Ni, and including multiple choices of surface structures, with comparison to experiments that mostly involved molecular beam measurements. The choice of functional that led to the best correlation between theory and experiment changed in the second paper compared to the first, with the

workhorse GGA functional PBE and the MS2 meta-GGA functional showing up as the most accurate in the most recent study. Here, GGA refers to the generalized gradient approximation, PBE is the Perdew Becke Ernzhof functional and MS2 is the Made Simple 2 functional. The mean absolute error in the PBE barriers was 2.4 kcal mol^{-1}. Furthermore, the results for functionals with parameters trained on adsorption thermochemistry were not superior to functionals with no training. This reveals the complexity of developing methods that properly cover a wide range of bonding interactions (covalent, ionic, and dispersion).

For the global PESs, we mention a recent review by Guo, who discusses machine-learning methods for both gas-phase and gas–surface reactions,[60] and a paper by Stark *et al.* that examines hydrogen on metals.[61] The Guo paper considers neural-network and Gaussian process regression approaches—as well as the PIP-NN mentioned above, including an application of this approach to gas–surface systems—that incorporate permutational symmetry in the "gas" part, and periodicity in the surface part. If the surface is rigid, this method works well. However, if it is not, an attractive alternative is to use the atomistic NN method of Behler and Parrinello,[62–64] in which the PES is expressed as a sum of atomistic contributions, each encoded by mapping functions that describe the local environment. Another useful paper is by Zhang *et al.* concerning the Shepard interpolation method as applied to molecule–surface systems.[65] Here the "Grow" method[66] for combining BOMD trajectories that include local Hessians with potential energy interpolation based on the Shepard method is generalized to include periodic boundary conditions, so that the underlying symmetry of the crystalline surface is included. Applications of this method to the H_2 molecule interacting with fcc(111) and hcp(0001) metal surfaces were considered.

One difficulty with machine learning arises when training data are limited. Here, the neural network may produce unphysical values of the PES that must be searched for and retrained. An alternative to ML is the use of physically realistic fitting functions, for example effective medium theory, which has been successfully applied to generate full-dimensional potentials for H interacting with metals.[67–69] The fitting error is typically larger with this approach, but the PES remains physically constrained. This is analogous to a Lennard-Jones potential for a diatomic molecule, which is less accurate than a spline function, but will not yield unphysical energies.

2.2. High-dimensional quantum dynamics

2.2.1 Gas phase. General reviews of quantum scattering for bimolecular systems have been published in many places, including a review of reactive scattering for the years 2007–2016 by Zhang and Guo,[70] and a review of studies of reactions with more than three atoms by Zhang[71] in 2018. There have also been reviews of specific quantum scattering methods, including two reviews of split-operator wave-packet methods by Sun and coworkers;[72,73] a review of wave-packet methods by Balint-Kurti;[74] a review of wave packets in Jacobi coordinates by Zhang, Sun and Guo;[75] and a review of wave packets in hyperspherical coordinates by Sun.[76] Also, Clary has reviewed the use of reduced-dimension quantum scattering methods for reactive collisions,[77] and Meyer has reviewed the MCTDH (multiconfiguration time-dependent Hartree) approach.[78] Note that MCTDH and its extensions provide a general method for dynamics calculations

that describe more degrees of freedom in reactions than can be considered with other methods in common use in the reaction dynamics field.[79]

While most of the methods reviewed above were originally developed long ago, the technology for carrying out scattering calculations continues to be developed. For example, Zhao *et al.* have described the use of wave packets that start near the transition state of a chemical reaction, but which can be used to calculate state-to-state reaction probabilities,[80] and DuPuy *et al.* have described Smolyak representations with absorbing boundary conditions for use with a reaction-path Hamiltonian model of reactive scattering.[81]

2.2.2 Gas–surface. Theoretical studies of the collisions of atoms or small molecules with surfaces leading to reactions are important to several processes in catalytic reactions. In spite of the complexity, there has been a lot of activity in this field, with reviews by Kroes and coworkers that describe methods for carrying out the calculations,[82] especially concerning dissociative chemisorption,[83] and including comparisons of quantum and classical descriptions of the reactive-scattering process.[84] Here, the focus of attention has been on collisions involving metallic surfaces, but there has also been interest in collisions of gases with organic liquids[85] and ionic liquids.[86] MCTDH is also important for gas–surface scattering—recently, fully quantum scattering calculations were demonstrated, involving 75 degrees of freedom and using a neural-network PES.[87] Another new development in this field has been the emergence of RPMD methods for describing gas–surface dynamics, such as recent work by Guo and coworkers,[88] who have studied H_2 dissociative chemisorption on Ag(111) and Pt(111), where this trajectory-based approach provides an easy way to study quantum effects related to tunneling over the dissociative barrier. Also, Li *et al.*[89] have used RPMD to determine the rate of desorption of NO from Pd(111), where it is possible to include anharmonic effects and barrier re-crossing in the dynamics.

2.3. Electronically non-adiabatic dynamics

Nonadiabatic effects resulting from the presence of many coupled PESs are very common in gas-phase collision processes, as many of these processes involve atoms or molecules with open-shell character (*i.e.*, that's what makes the species reactive). As a result, the development of PESs and methods for simulating the dynamics has often focused on generating multiple surfaces and on determining their couplings, where the couplings can involve either derivative coupling of adiabatic surfaces, or spin–orbit coupling that leads to intersystem crossing. Among the recent studies in this area is a paper by Kendrick in 2018, concerned with the description of quantum reactive scattering using hyperspherical coordinates that includes many surfaces and nonadiabatic effects.[90] Also, Meuwly in 2020 provided an overview of methods for describing dynamics involving multiple PESs,[91] including a detailed description of surface-hopping methods for describing nonadiabatic dynamics.

Studies on the impact of multi-surface and nonadiabatic effects on the dynamics of gas–surface reactions have mainly been focused on friction models arising when nuclear motions are coupled to a continuum of electronic states that are present when a molecule interacts with a metal surface. Recent work includes studies by Kroes on hot-atom relaxation in the H + Pd(100) system[92] and in N_2 dissociative chemisorption on Ru(0001).[93] Also, Guo has studied frictional effects

in H_2 scattering from Ag(111).[94] The Guo work describes the inclusion of friction effects in terms of a generalized Langevin equation, in which there is an electronic friction tensor that is determined by Fermi's golden rule based on derivative couplings and an empirically chosen delta function to smooth out the k-state interpolation. In addition, the friction tensor is represented as a function of nuclear coordinates using a NN approach, which requires special care because of the dependence of this tensor on the molecular coordinate directions.

In gas–surface interactions, a local density friction approximation is often used;[95] this approach often works well for nonadiabatic energy transfer in atom scattering from metals.[92,96] Recently, tensorial electronic friction methods have been more extensively elaborated.[97,98] Friction tensors can also be represented by neural networks[99] and show great promise for describing nonadiabatic interactions of molecules with metal surfaces.[100,101]

3. Advances in experimental methods

Scattering methods are sensitive probes of the microscopic world, as exemplified by one of the most famous experiments of the modern era of physics, the α-particle scattering from gold foil by Rutherford,[102] which helped establish the structure of the atom, thereby laying the foundation for theoretical chemistry. In an analogous way, molecular beam scattering methods have been essential for the study of reaction dynamics in both gas–gas and gas–surface collisions. In such experiments, the kinetic energy and angular distributions of scattered atoms and molecules are measured; these distributions contain detailed dynamical information that can be used to understand chemical reactions in gas-phase or gas–surface interactions. The two key capabilities needed for molecular beam scattering methods are: (1) the production of intense atomic or molecular beams and (2) methods for sensitive detection of atoms and molecules. Over the last few decades, great experimental advances have been achieved, allowing much higher energy and angular resolution and more sensitive detection.

Since the development of the original universal crossed-molecular-beams method[29]—see above—many improvements have been demonstrated. For example, dramatically improved vacuum in the universal detector chamber was achieved using state-of-art vacuum techniques. This further lowered the detector background and thereby enhanced the detection efficiency.[103] Further development of the crossed universal beams method has employed different ionization methods, such as tunable VUV synchrotron ionization,[104] VUV laser ionization[105–107] and soft electron-impact ionization.[108] These techniques have provided powerful tools to study the dynamics of both elementary and complex chemical reactions.

Molecular detection based on laser ionization and ion imaging has revolutionized scattering experiments. While resonance-enhanced multiphoton ionization (REMPI) had been developed already in the 60's and the 70's,[109–118] it was only in the mid 90's that it was combined with molecular beams to provide product speed and angular distributions.[119] Ion imaging was quickly applied to products of both photodissociation[120] as well as bimolecular reactions[121,122] and became even more attractive when velocity-map imaging (VMI)[123] demonstrated enhanced resolution, comparable to that of the Lee style rotating mass spectrometric detector. With the advent of "slice imaging" in 2001,[124] symmetry requirements for image data analysis could be circumvented, and over time, this

approach has become the method of choice for many problems in chemical dynamics.[125–127] Recently, a two-photon near-threshold ionization scheme for H atoms was applied in the H + HD reaction, and high kinetic and angular resolution for hydrogen atom product imaging was achieved.[128] The most modern variations of this include covariance imaging[129] and pixel imaging mass spectrometry.[130] These techniques allow analysis of complex polyatomic dissociation events *via* the identification of momentum-matched dissociation partners. It is not an exaggeration to say that ion imaging is the most important experimental development since the universal crossed-beams method.

Another important experimental method developed for crossed-molecular-beam scattering study is the H-atom Rydberg tagging time-of-flight (HRTOF) technique, which provides very high kinetic-energy resolution. This technique was developed by Welge and co-workers,[131,132] who also employed laser photolysis of HI to produce nearly monoenergetic H atoms with tunable kinetic energy for studying the H + D_2 reaction,[133] and it has been widely applied in the study of elementary chemical reactions[134–139] as well as photodissociation dynamics studies of molecules with H-atom products.[140–142] The central scheme of this technique is the two-step excitation of the H-atom product from its ground state to a long-lived high-*n* Rydberg state without ionization. The Rydberg "tagged" neutral H atoms are not influenced either by space charge or stray fields, and after a certain flight distance, they are easily field-ionized and the time-of-flight (TOF) spectrum is recorded using microchannel plates. The method's unique combination of high resolution and high sensitivity makes it particularly powerful in providing detailed quantum dynamical information on benchmark elementary chemical reactions and it is able to detect subtle quantum phenomena in chemical reactions, such as reaction resonances, spin–orbit dynamics effects, and geometric phase effects.

Great progress has also been made in developing intense and high-quality atomic and molecular beams for crossed-beams scattering experiments and gas–surface scattering experiments. These include, for example, photolytic and discharge radical beam sources of H,[143] C,[144–146] O(^{3}P,^{1}D),[147] F,[148] Cl,[149] $^1CH_2$,[150] C_2,[151,152] C_3,[153] C_2H,[154] OH,[147] CN,[155] NCO,[156] and CH_3 and phenyl radicals.[107]

Our ability to control the beam's translational energy has also improved enormously. On the low-energy side of things, polar molecules can be brought nearly to a standstill,[157] whereas on the high-energy side, fast O-atom sources with speeds of more than 8000 m s^{-1} can be generated with laser detonation sources.[158,159] This wide range of beam speeds allows us to study reaction dynamics at extremely low temperatures near absolute zero or at temperatures of more than 10 000°, extending experimental studies of reaction dynamics to extreme environments, such as the interstellar media and hot rocket plumes.

Molecular beams of stable species with vibrational excitation have also been developed, which allows investigation of the effects of vibrational excitation on gas-phase chemical reactions as well as gas–surface reactions.[160–164] Oriented molecular beams of NO,[165] and aligned methane[166,167] and hydrogen (HD) molecules[168,169] in vibrationally excited states, can also be prepared for studies of steric effects in reactive scatterings. The optical preparation of small molecules for scattering experiments is in itself a broad field that goes beyond the scope of this paper.

4. Simple systems in gas-phase scattering

In this section, we provide some benchmark examples of crossed-beams scattering studies of both triatomic elementary and complex reactions. Here, the simplicity of the systems is such that essentially exact theoretical calculations are possible; in fact, the experiments are of such high quality that this can be demonstrated. Combining theory and experiment leads to some remarkable conclusions about quantum mechanical reactivity.

4.1. The H + H_2 reaction: searching for the geometric phase effect

The H + H_2 → H_2 + H reaction (along with its isotopic variants) has been one of the most important bench-mark systems for studies of quantum dynamics in chemical reactions[133,136,170–172] and these reactions have provided a key testing ground for developing a quantum dynamical theory and understanding quantum phenomena in chemical reactions. Experimentally, this reaction has been studied using all three major crossed-molecular-beams scattering methods. Lee and coworkers used the universal crossed-molecular-beams method to obtain differential cross sections for the D + H_2 reaction.[173] The Rydberg atom-tagging technique has played a particularly important role.[132,133,135,137,139,170,174] This reaction system has also been studied using the ion imaging technique.[122,175,176] The recent experimental studies on this reaction have provided an accurate reactive-scattering picture of this system for detailed comparisons with quantum-dynamics calculations.

Some of the first theories of chemical reactivity were developed based on these reactions, first employing a co-linear model in the 1970s,[177] and subsequently, three-dimensional quantum-dynamics calculations were performed.[35,178] Since then, many dynamics calculations have been carried out and over the years, and quantitative agreement between theory and experiment has been reached for the dynamics at low collision energies. This laid the foundation for quantitatively understanding the quantum reaction dynamics of this reaction, especially the dynamics of bottleneck transition states in chemical reactions.[179,180] Ever-improving scattering experiments and exact quantum-dynamics calculations based on highly accurate potential energy surfaces have driven our understanding of the dynamics of this reaction to new heights.

The interplay between experiment and theory led to the direct observation of the geometric phase (GP) effect in this reaction,[181] which describes the quantum influence of the conical intersection on the reaction, *i.e.*, including a vector potential that describes the phase acquired when a quantum state is adiabatically transported around a conical intersection when calculating the overall scattering cross section.[182] Great efforts in both theory and experiment have been made in this direction.[170,183–188] Accurate quantum-dynamics calculations helped guide experiment, showing that the GP effect is negligible at total energies below 1.6 eV[188–193] but could be significant at high collision energies.

In 2018, a high-resolution crossed-beams imaging study on the H + HD → H_2 + D reaction was performed at a collision energy of 2.77 eV. This unambiguously revealed evidence of the GP effect, which could be found in the H_2 product state-resolved angular distributions.[175] Fig. 1 shows the experimental image of the D products from this reaction. Comparison to quantum-dynamics calculations showed that the observations could only be quantitatively reproduced when the

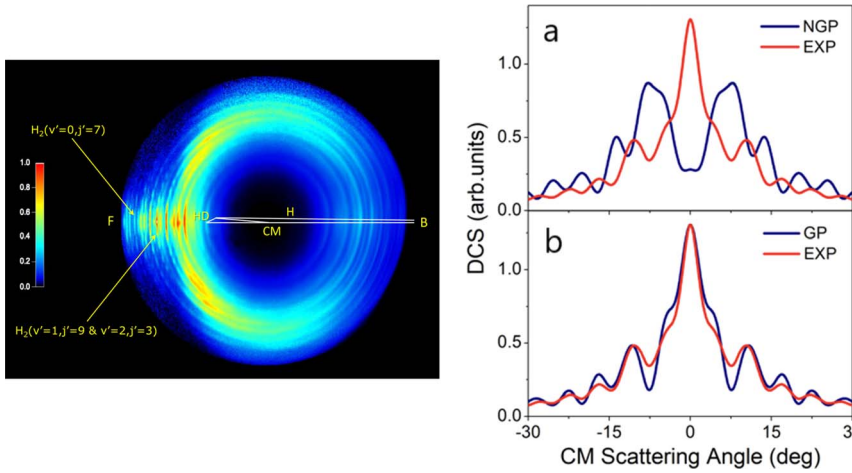

Fig. 1 (left panel) Experimental image of the D-atom product from the H + HD → H_2 + D reaction at a collision energy of 2.77 eV. "F" and "B" represent the forward (0°) and backward (180°) scattering directions, respectively, for the H_2 co-product in the center-of-mass frame relative to the H-atom beam direction. Oscillatory structures in the forward scattering direction are observed for H_2 product in specific quantum states—these oscillations reflect interference generated by the geometric phase effect in the reaction. (right panels) Comparisons between the experimental (EXP) and theoretical product angular distributions: (a) NGP, not including the geometric phase effect; (b) GP, including geometric phase effect for the H + HD ($v = 0, j = 0$) → H_2 ($v' = 0, j' = 7$) + D reaction at 2.77 eV. Adapted from ref. 175 and used with permission under lic. no. 5744150372346.

GP effect was included. The GP effect could be shown to arise from the quantum interference between a direct abstraction channel and an insertion type channel (see Fig. 2) possible at high energy, which is topologically different—that is, it involves a pathway that passes around the conical intersection. The close interplay between theory and experiment was essential, not only to push the understanding of the reaction dynamics to an unprecedented level, but also for the discovery of the geometric phase effect in chemical reactions.

4.2. The F + H_2 reaction: probing reaction resonances

The F + H_2 → HF + H reaction has also proven to be one of the most important systems for studying quantum mechanical reaction dynamics. In particular, it exhibits reaction resonances, which have attracted great attention over the last forty years. Reaction resonances were first proposed in the quantum-dynamics calculation of the F + H_2 reaction based on a collinear model[194,195] and the first crossed-molecular-beams study of the F + H_2 reaction was performed with product vibrational state resolution in 1984. An unexpected forward-scattering peak for the HF ($v' = 3$) product was observed while HF ($v' = 1, 2$) products were found to be backward scattered. The forward scattering peak was attributed to a reaction resonance.[196] Due to a lack of adequate theory at the time, an unambiguous determination of the physical origin of this forward scattering was not possible.[197,198] In 2000, a clear step-like structure was observed in the collision-

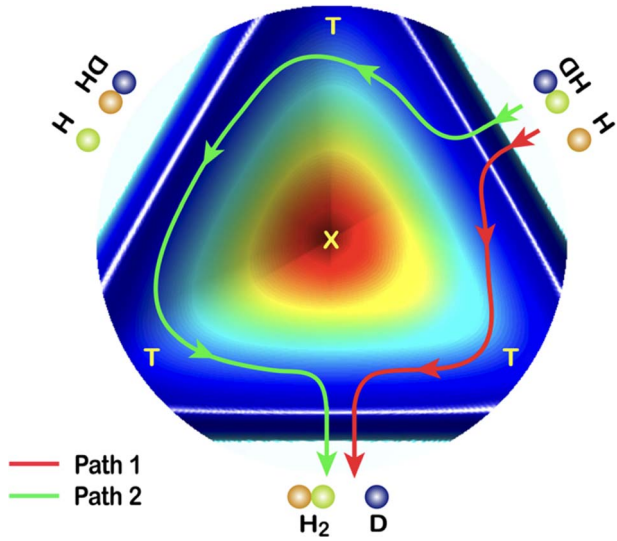

Fig. 2 A cut view through the H + HD potential energy surface with transition states (T) and conical interaction (X). Two representative reaction pathways are shown: a one-transition-state reaction path (Path 1) and a two-transition-states reaction path (Path 2). Adapted from ref. 175 and used with permission under lic. no. 5744150372346.

energy-dependent integral cross section in F + HD → HF + D and assigned to a quasi-bound quantum resonance.[199]

Over the last couple of decades, improved experiments have become possible using the H-atom Rydberg-tagging technique with full product rotational and vibrational state resolution.[200–203] These data provide unprecedented detail and require a close collaboration with highly accurate quantum dynamical theory. Through this cooperative approach, a spectroscopically accurate physical picture for reaction resonances has emerged and shows clearly that they reside in the post barrier region. The resonance states are quasi-bound quantum states in the transition-state complex of the vibrationally excited HF molecule bound to an H-atom (see Fig. 3). Excellent agreement was also reached between the crossed-beams scattering experiment and negative-ion photodetachment studies.[201,204,205] It is noteworthy to point out that reaction resonances demonstrated so clearly in the F + H_2 reaction also exist in many other systems, suggesting that reaction resonance is not a rare phenomenon in chemistry. It is obviously more general than we have realized previously.

The fluorine atom exhibits two spin orbit states, offering an opportunity to investigate the spin–orbit effect on this reaction. Recently, high-resolution velocity-map ion imaging was performed on the F($^2P_{3/2}$) + HD → HF + D reaction and a peculiar horse-shoe pattern in the scattering differential cross section was observed at a collision energy of 2.10 kcal mol^{-1}.[206] This was attributed to quantum interference between spin–orbit split-partial-wave resonances in this reaction, suggesting that spin–orbit interaction has a significant influence on the detailed dynamics of this resonance-mediated chemical reaction.

In this section, we have provided examples of dynamics studies of two important elementary reactions: the H + H_2 reaction and the F + H_2 reaction.

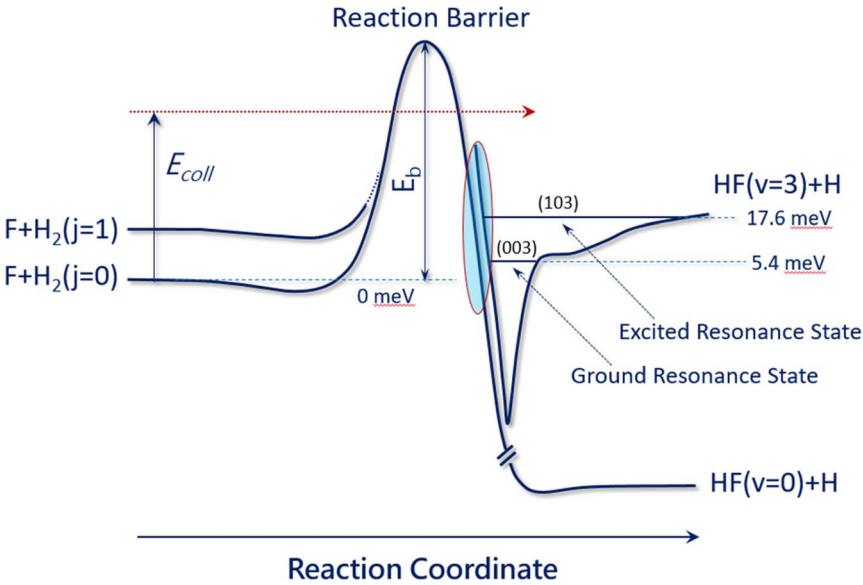

Fig. 3 Reaction resonances in the F + H_2 reaction. This figure presents the accurate physical picture of the quantum resonances in the F + H_2 ($j = 0$) and F + H_2 ($j = 1$) reactions, resembling a vibrationally excited HF molecule in the presence of an H atom. Two resonance states reside in the exit channel: the ground resonance state (003) at 5.4 meV is mainly responsible for the F + H_2 ($j = 0$) reaction at temperatures below 40 K, while the excited resonance state (103) at 17.6 meV plays a more important role for the F + H_2 ($j = 0$) reaction at temperatures above 40 K (adapted from ref. 200).

Many more simple elementary reactions like these have also been investigated, for example, Cl + H_2,[207–209] $C(^1D)$ + H_2,[210] $O(^3P)$ + H_2,[211] $O(^1D)$ + H_2,[212,213] $N(^2D)$ + H_2,[214] and OH + H_2 (ref. 134 and 215), to name a few of the most important ones. Experimentally, full differential cross sections of the scattering dynamics of these elementary chemical reactions can be measured over a wide collision energy range with full quantum-state resolution. Theoretically, the advancement of efficient quantum-dynamics methods and rapidly growing computing power now makes accurate calculations of the reactive-scattering dynamics possible. The close interplay between theory and experiment has greatly enhanced our understanding of the quantum dynamics of elementary chemical reactions, especially for reaction resonances and geometric phase effects.

It is now possible to say with confidence that quantum theory of chemical reactions has advanced to a quantitatively accurate level, especially for reactions involving only the ground electronic state. Many simple elementary reactions, like those mentioned above, can in fact be studied using theoretical tools with high accuracy. Precise reactive-scattering experiments are often used as the ultimate testing ground for further developing quantum theory of chemical reactions to even higher levels of accuracy. The successes of quantum theory in elementary chemical reactions give us high confidence to seek quantitative understanding of more complex and challenging problems, to which we now turn.

5. Dynamics of more complex gas-phase reactions

In this section, we describe selected studies on gas–gas collision dynamics where the cooperative interaction of theory and experiment is essential to successful outcomes. This cooperative approach allows much more complex problems to be tackled than ever before, providing quantitative outcomes that in some cases can even be used to support engineering efforts on practical real-world problems.

5.1. Crossed-beams scattering

Although initially used to target the simplest reactions, crossed-molecular-beams scattering has proven to be a powerful tool for studies of polyatomic reactions, often providing a deep understanding of the dynamics and mechanisms of complex chemical reactions.[108,216] Using sliced velocity-map ion imaging to measure the state-resolved differential cross section for CD_3 products from F + CD_4 → DF + CD_3, Liu and coworkers[217,218] demonstrated that vibrational state-resolved, pair-correlated information can be obtained. Striking differences in the correlation between different product state pairs could be detected, indicating the complexity of polyatomic reactions. An interesting reaction resonance phenomenon was also observed.[219] Crossed-beams reactive-scattering studies on F + CHD_3 → HF + CD_3,[220,221] F + CH_4 → HF + CH_3,[222] Cl + CH_4 → HCl + CH_3,[223] Cl + SiH_4 → HCl + SiH_3,[224] and F + SiH_4 → HF + SiH_3 [225] have also been carried out and vibrational state pair correlated information could also be acquired. In the study of the H + CD_4 reaction, a depression in the reactivity of H + CD_4 → HD + CD_3 by collision energy was observed.[226]

The power of combining experiment and theory could also been seen in a study on the $O(^1D)$ + CHD_3 → OH + CD_3 reaction.[227] This reaction has long been thought to be the prototypical example of collision-complex formation that occurs by direct insertion of the O atom into a C–H bond. Such reactions are expected to exhibit forward–backward symmetry in the center-of-mass angular distributions. It was therefore a puzzle to understand why this reaction exhibited strong forward scattering in state-resolved ion imaging measurements of the CD_3 products. Using an accurate full-dimensional PES, quasiclassical trajectories were able to reproduce the forward scattering and demonstrated that the "insertion reaction" is essentially a two-step process where abstraction products (OH + CD_3) remain bound to one another long enough to rotate into position to form a C–O bond, thus producing the hot methanol "insertion" complex. The dynamics discovered here were called trapped abstraction and are thought to be important in many reactions currently named insertion reactions.

A major issue in studying the bimolecular chemistry of larger systems is evaluating the branching between the many possible product channels and understanding the dynamical mechanisms that produce them. An excellent example is the reaction of $O(^1D)$ with CH_4 studied using an improved universal crossed-molecular-beams apparatus with an ultrahigh-vacuum detector ($\sim 1 \times 10^{-12}$ torr).[228] Three different reaction channels have been detected: the OH + CH_3 channel, the CH_2OH/CH_3O + H channel and the $H_2CO/HCOH$ + H_2 channel. Note that the crossed-molecular-beams method does not necessarily yield information about which product isomers are formed. Interestingly, the dynamics of the three

channels appear to be quite distinctive. The OH + CH_3 products appear to be forward scattered, and the CH_2OH/CH_3O + H channel is slightly backward scattered, while the $H_2CO/HCOH$ + H_2 product angular distribution is almost isotropic. It is interesting to see that the three channels in the same reaction appear to have quite different dynamical behaviors.

As the reactions involve more and more atoms, the crossed-beams method has been augmented with important experimental improvements. For example, using low-energy electrons for electron-impact soft ionization, dissociative ionization can be suppressed. When this is successful, each measured mass-to-charge ratio indicates the mass of the detected product. This has proven to be a powerful tool for analyzing more complex reactions. For example, five different reaction channels have been detected and studied in the reaction of $O(^3P)$ with C_2H_2.[229]

In the even more complex reaction of $O(^3P)$ + C_3H_4 (allene), this approach has been able to identify and quantify four reaction channels forming C_2H_4 + CO,

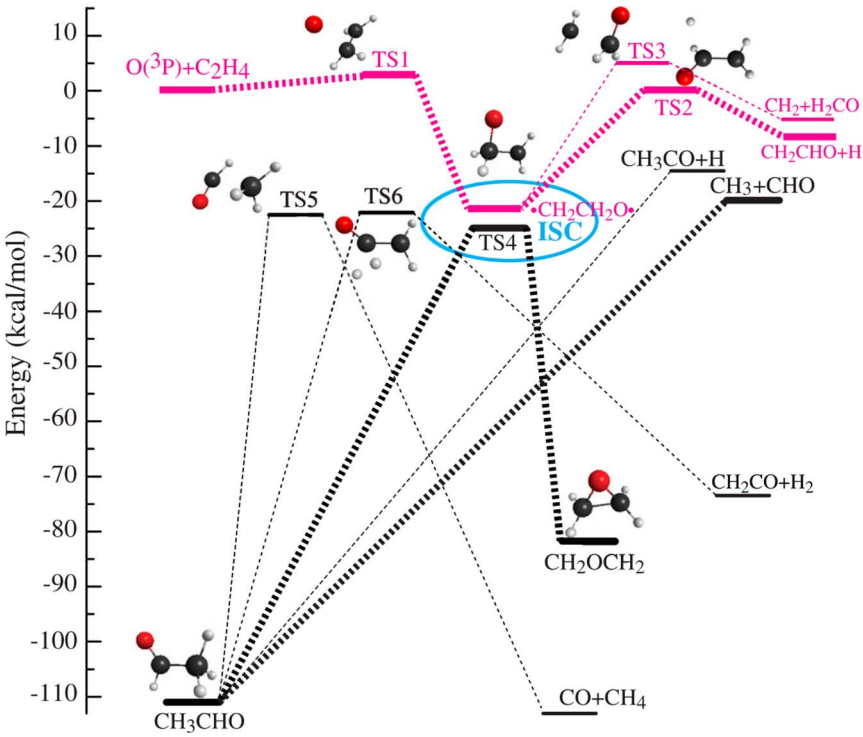

Fig. 4 Simplified schematic of triplet (red) and singlet (black) potentials of the $O(^3P)$ + C_2H_4 reaction. The electrophilic oxygen atom attacks the C=C bond through a very low barrier of about 3 kcal mol^{-1} and forms an energetic triplet biradical, $^{\bullet}CH_2CH_2O^{\bullet}$. The biradical region, enclosed by the ellipse, is where intersystem crossing (ISC) takes place with the greatest probability. ISC competes with fragmentation and rearrangement. The corresponding singlet biradical can isomerize to acetaldehyde (CH_3CHO), which subsequently dissociates because of its high energy content. The triplet biradical can dissociate to H + CH_2CHO or to CH_2 + H_2CO. The singlet biradical can also isomerize to oxirane *via* oxygen migration and ring-closure. The oxirane will finally isomerize to CH_3CHO and further dissociate from CH_3CHO into various products, CH_3 + HCO, and H + CH_3CO. Adapted from ref. 230.

$C_2H_2 + H_2CO$, $C_2H_3 + HCO$, $CH_2CCHO + H$, and $CH_2CO + CH_2$. Because some of the observed products can only be formed *via* intersystem crossing (ISC) from triplet to singlet potential energy surfaces, the breakdown of spin conservation in this reaction could be inferred. The product branching ratios indicate that fully 90% of the reactive events proceed through ISC.[231] ISC has since then been identified as an important aspect of the mechanisms of the reactions of $O(^3P)$ with ethene,[230] pyridine[232] and 1,3-butadiene.[233] In the simplest of these (see Fig. 4) surface-hopping trajectory calculations could be performed using two full-dimensional PESs (singlet and triplet) to investigate the ISC dynamics more directly. Excellent agreement between experiment and theory demonstrated theory's ability to describe complex multichannel nonadiabatic reactions.

In general, the application of theory in combination with crossed-molecular-beams experiments has led to fundamental understanding of quite complex reactions.[234–251] The impact of modern scattering on real systems can be exemplified in the studies of $O(^3P) + C_6H_6$ (benzene). Here, a theoretical statistical approach could be validated by comparison to the crossed-molecular-beam results and subsequently used to compute channel-specific rate constants as a function of temperature and pressure.[252] Such rate constants are essential to microkinetic models of combustion and atmospheric chemistry.

Crossed molecular beam scattering experiments have also been applied to problems in interstellar and planetary chemistry.[146,253–258] An excellent example of this is the reaction of $N(^2D)$ with benzene.[259] Theory shows that the atom adds to the benzene ring and after isomerization can form several cyclic and linear intermediates, which undergo unimolecular decomposition. With the help of theory, it could be clearly shown that the dominant channel forms the ring-contracted C_5H_5 cyclic radical along with HCN and that formation of HNC is negligible. Note that the experiment is incapable of distinguishing HCN from HNC, as only the mass-to-charge ratio is determined.

Crossed molecular beam studies of reactions of transition-metal atoms with hydrocarbons is another exciting area of modern scattering research, providing mechanistic and dynamical information about inorganic reactions.[260–277] This has been made possible by laser vaporization sources for transition-metal atom beams that have been developed for, among others, Mo, Y, Zr, Nb, and Al.[260–265] State-selected and electronically excited Mo atoms can be produced by laser excitation followed by radiative relaxation, resulting in the reaction $Mo(^5S_2) + CH_4 \rightarrow MoCH_2 + H_2$.[265] The competition between C–C and C–H bond insertion was studied with experiment and theory for cyclopropane[270,271] and propene[271] and four butene isomers,[272] as well as alkynes.[272] When methane was vibrationally excited with a laser, yttrium atom insertion into the C–H bond was enhanced by at least a factor of two.[274]

5.2. Ions and electrons in crossed-beams experiments

The crossed molecular beams method using ion imaging has also been applied to ion–molecule reactions, providing great insights into textbook reaction mechanisms.[278] For example, the S_N2 mechanisms for ion exchange could be studied in the reaction of $F^- + C_2H_5Cl \rightarrow Cl^- + C_2H_5F$. Measured angle- and velocity-differential scattering cross sections were compared with quasiclassical trajectory simulations carried out on a full-dimensional PES, and quantitative

agreement was found. The anti-E2 pathway turned out to be most important, but the S_N2 substitution pathway became more relevant at higher collision energy.[279]

Another interesting direction uses ion imaging to study electron–molecule collisions. Electron bombardment ionization has long been one of the most important detection techniques for molecules, yet the underlying physical chemistry has not been thoroughly understood. Recently, this process has been studied using ion imaging in a crossed-beams geometry.[280–285] The use of pixel imaging mass spectrometry and covariance imaging allows identification of fragments arising from the same parent ions and detection of doubly charged ions on a large background of singly charged ions.[281] This is particularly useful when analyzing the fragmentation patterns of larger polyatomic molecules and provides accurate observations of the decomposition channels that occur in the violent ionization event.

5.3. Cold collisions

In 1997 a rather overlooked paper appeared, describing calculations of the motion of a dipolar molecule within an electrostatic trap.[286] The calculations were based on precisely measured Stark shifts in fields up to 140 kV cm^{-1} for the doubly degenerate ($v = 0, J = 1$) level of metastable CO ($\tilde{a}^3\Pi$). This paper described the basic physics that launched the emerging field of cold collisions.[287–291] What the authors had realized and demonstrated with their model calculations was that it was possible to manipulate the velocities of molecules with external electric fields, especially if one concentrated on slow-moving dipolar molecules with near-degenerate low-field-seeking states; that is, those exhibiting a 1st order Stark effect. This was the secret-sauce added to the original recipe of Auerbach and Wharton, who had, years earlier, developed ideas to use the Stark effect to accelerate molecules.[292] In a breathtakingly short span of time, deceleration of molecules was demonstrated in the laboratory,[293] as was phase-stable confinement in a travelling trap,[294] and a storage ring was built and characterized.[295] These extraordinary new tools were followed by additional inventions, like a molecular synchrotron[296] and a trap on a chip.[297] Meanwhile, other methods for decelerating and trapping atoms and molecules were being developed, like the coherent paddle,[298] the magnetic coil gun[298,299] and the Zeeman decelerator.[300,301] The lesson had been learned. If one were to choose specific states of atoms and molecules that exhibited optimal magnetic or electric properties, one might exploit those properties to produce decelerated beams with tunable velocities. Such states could be found as the ground state of a few molecules, but with discharges and laser excitation, even more possibilities came into view in the form of excited states.

It was clear from the outset that these new techniques would be important for molecular scattering, promising to reveal subtle nuclear quantum effects that had never before been seen. Putting Stark decelerated molecules to work for this purpose was accomplished early on, in a crossed-beams configuration for OH scattering from Xe,[302] D_2 [303] and Ar.[304] Considerations about how to achieve optimized energy resolution, with an eye toward seeing collision resonances, were also reported.[305] Another innovation was the merging of two nearly perfectly co-propagating molecular beams and 3D printing methods were developed to help fabricate the complex structures needed for the electrodes.[306] Merged beams

allowed extraordinarily low incidence energies and high energy resolution to be achieved in collisions. The energy resolution was, in fact, now so high that optimized VMI detection needed to be developed to take full advantage of it.[307]

With all of these wonderful tools in place, new observations were guaranteed. By scanning the collision energy, reaction resonances were detected for Penning ionization[308–311] and rotationally inelastic collisions.[312] A key element of these observations followed the pioneering work on $F + H_2$ reaction resonances seen at much higher energies;[202,313] as in that work, by obtaining the incidence-energy dependence of a small angular fraction of the differential scattering angular distribution, the resonances could be directly seen. While this was not the first observation of resonance behavior in molecular scattering, these new methods allowed resonance line shapes to be measured with unprecedented ($\sim$1 cm^{-1}) energy resolution, from which resonance lifetimes could be experimentally derived.[314] With the help of theory and by comparing integral to differential scattering cross sections, the contributions of individual scattering waves could be determined.[315] In analogous work, HD rotational energy transfer with H_2 and D_2 was examined at low collision energy with bond axis orientation and evidence of resonances sensitive to the anisotropic interaction between molecules was found.[316] First-principles simulations of these experiments identified the $L = 2$ partial wave engaging in a shape resonance as being responsible for the observations.[317] This showed once again how valuable it can be to resolve partial waves when searching for evidence of scattering resonances.

Other fascinating quantum phenomena have since been observed in molecular scattering. This includes diffraction scattering[318–320] and the transition at low incidence energies from Langevin capture scattering to Wigner scattering.[321] Taking advantage of the high energy resolution, quantum-state correlated scattering could also be achieved.[320] Illustrating the analogy to high-precision molecular spectroscopy, experimental and theoretical comparisons for NO scattering with H_2 were able to validate one PES *versus* another, even though the binding energies between the two differed by only 2 cm^{-1}.[322]

5.4. Low-temperature kinetics

The inspired ideas of this field also led to a creative new approach to study ion–molecule chemistry at extraordinarily low temperatures, where the reaction is observed within the orbit of a Rydberg electron.[323] Using external fields, the Rydberg atom's velocity could be controlled[324] and when matched to the speed of another merged beam, reaction conditions that simulate a temperature near 0 K could be achieved. This provided a special approach to studying state-resolved capture probabilities. In one example, reactions of $He^+ + CH_3F$ forming CH_2^+ and CHF^+ were observed and a large enhancement of the reaction probability was seen below a collision energy of 1 K. This was explained by a state-resolved capture model involving low-field-seeking states of the CH_3F molecule becoming favorably oriented for reaction within the electric field of the He^+.[323] This reaction model was also able to explain the more complex behavior exhibited by the reaction of He^+ with NH_3 forming NH_2^+ and NH^+.[325] Using isotopic labeling, it could be shown that the reactivity of high-field-seeking states of ammonia exhibiting a 1st-order Stark effect increased dramatically at low collision energy. High-field-seeking states with a 2nd-order Stark effect were less strongly reactive,

while the reactivity of low-field-seeking states became suppressed. State-resolved electrostatic influences on the reaction $He^+ + CO \rightarrow He + C^+ + O$ were also seen; here, CO's negative quadrupole moment suppresses reaction at low collision energy.[326] Other interesting insights were derived from studies of the reactions of He^+ with CH_4 [327] and N_2 [328] and NO.[329]

Understanding quantum effects in chemistry has importance far beyond the field of cold-collision physics. For example, quantum mechanical tunneling can be important in astrochemistry taking place in cold dense interstellar clouds.[330] This conclusion now supersedes the traditional viewpoint that reactions are unimportant in astrochemistry if they possess significant activation barriers. This is due to the fact that barriers can be overcome by tunneling, especially when gas-phase collisions first lead to reactant complexes bound by even weak van der Waals forces, as was shown first to be the case for the reaction $OH + CH_3OH \rightarrow H_2O + CH_3O$[331] and later for many other reactions.[330] Here, Laval nozzle expansions are ideal for producing low-temperature thermal conditions.[332]

For ion–molecule reactions, other methods are required—for example the tunneling contribution to the reaction of $H_2 + D^- \rightarrow H^- + HD$ could be determined *via* rate measurements at 10 K in a cryogenic 22-pole ion trap.[333] These are some of the smallest reaction rates ever measured and comparison to theory was essential to the conclusions of the work. It is however unusual that such accurate calculations of tunneling rates can be performed. Normally one relies on the observation of unusually large kinetic isotope effects to identify tunneling. Recently, it has been pointed out that more accurate multi-dimensional tunneling[334] and resonance enhancement[335] models of tunneling are needed to accurately characterize quantum mechanical rates in condensed phases.

This concludes our review of new directions in gas-phase molecular scattering. In the remainder of the review, we turn to a very different research area involving gas–surface scattering. Beam–surface scattering has been pursued nearly as long as beam–beam scattering. However, it has only been in recent years that challenges associated with instrumental complexity and the physical phenomena themselves have been slowly overcome. Here again, cooperation of theory with experiment is essential. Before entering into this broad and fascinating field, we note several prior reviews on gas–surface scattering dynamics.[336–347]

6. Simple systems in scattering from surfaces

Applications of *ab initio* dynamical theory to problems in surface scattering are nearly always subject to severe approximations, as has been outlined in Section 2. One is normally restricted to the use of DFT-GGA, and there are many atoms (degrees of freedom) involved, requiring the dynamics to be computed on high-dimensional PESs under the classical approximation. This means that in scattering from surfaces, the number of systems is small where the information gleaned from *ab initio* dynamical theory surpasses that obtained from experiment. Such systems do however exist.

6.1. H-atom scattering from simple surfaces

In comparison to other possible choices, H-atom scattering is simple and provides perhaps the best chance for current theoretical methods to be

implemented with the fewest possible approximations and with the highest accuracy. This motivated construction of a novel instrument, where nearly mono-

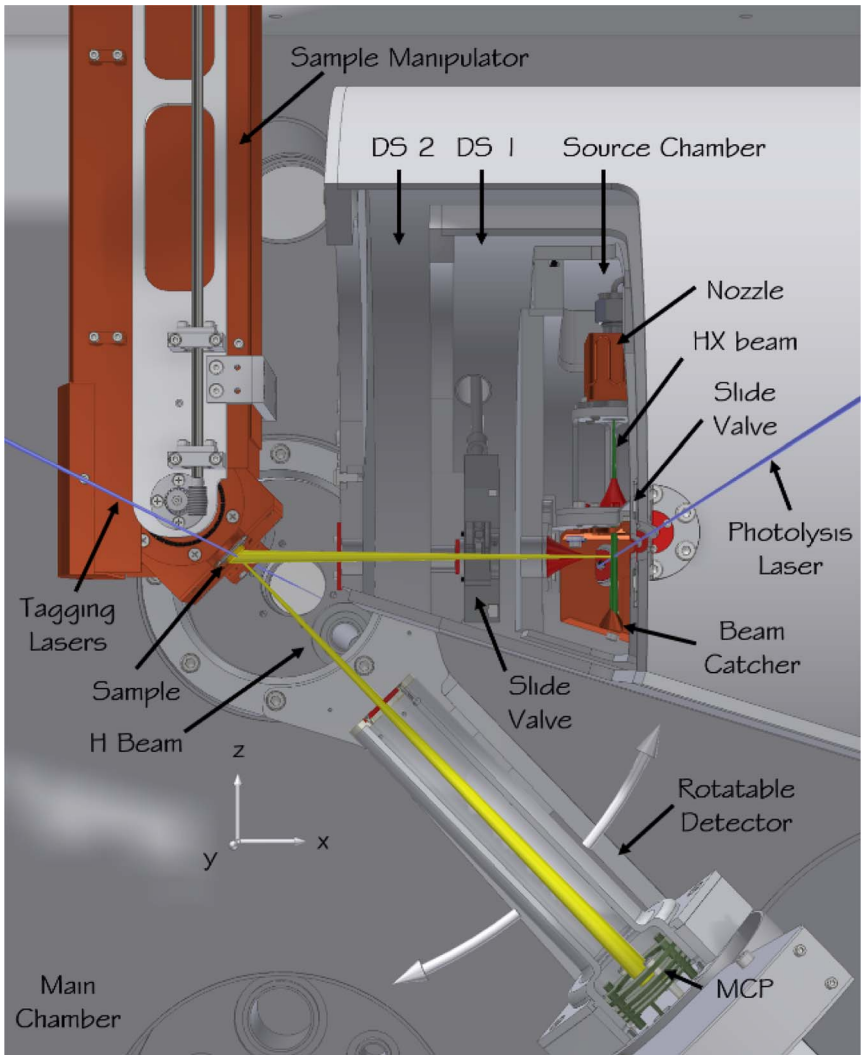

Fig. 5 Apparatus for scattering H atoms from pristine surfaces. In the source chamber, a hydrogen halide molecular beam (green) is formed in a supersonic expansion from a pulsed nozzle, passes a skimmer (red), and is intersected by the photolysis laser (blue) before it hits a liquid-nitrogen-cooled beam catcher. Some of the generated H atoms (yellow) leave the source chamber through a second skimmer, pass two differential pumping stages, and enter the main chamber where they collide with the sample surface. The sample is mounted on a six-axis manipulator allowing the incidence polar and azimuthal angles to be varied. The surface temperature can also be varied. The scattered H atoms are excited to a metastable Rydberg state by the tagging lasers, pass an aperture defining the angular resolution of the detector, and after a 250 mm flight path are field ionized and the ions are detected by a microchannel plate detector. The detector is mounted on a rotatable arm to enable variation of the scattering angle. The ultimate pressure in the scattering chamber can be reduced to below 1×10^{-10} torr. Adapted from ref. 348.

energetic H atoms could be scattered from clean and well-defined surfaces held in an ultrahigh vacuum and the incidence and scattering angle-dependent energy loss distributions could be measured with high resolution.[349] The experimental challenges involved in the execution of such an experiment are the production of near monoenergetic H atoms—achieved by laser photolysis of molecular beam cooled hydrogen halide molecules—and achieving high-resolution energy loss distributions, which is accomplished using Rydberg atom tagging as described in Section 3. Fortunately, these techniques had been previously worked out for gas-phase problems[133]—it was only necessary to adapt them to a UHV set-up.

A diagram of the H-atom surface scattering set-up is shown in Fig. 5;[349] work performed with this instrument has been recently reviewed.[348] H scattering has been performed from solid surfaces composed of metals,[350–355] adsorbate-modified metals,[356] semiconductors[357,358] and graphene[359,360] grown on a number of substrates.

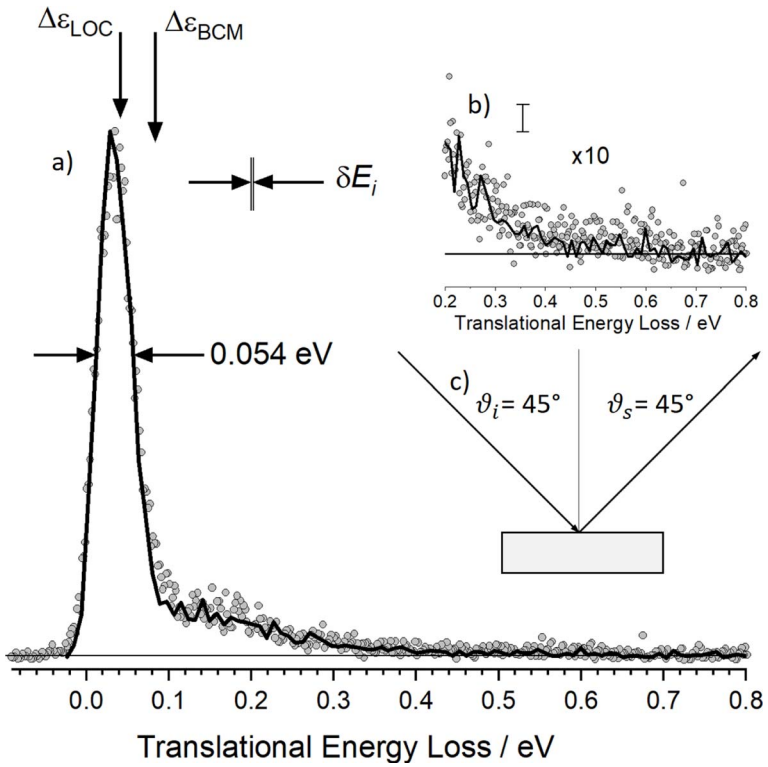

Fig. 6 Energy-loss spectrum for H scattering from solid Xe. (a) Rydberg tagging experiment (circles) and MD simulation (solid line). The sharp peak dominating the energy distribution results from single-bounce line-of-centers scattering and "weak double-bounce scattering". The shoulder spanning 0.1–0.5 eV results from strong double-bounce and multi-bounce collisions including subsurface scattering. The inset (b) shows a zoomed in view of the data with the largest inelasticity and an estimate of the statistical noise in the MD trajectories. (c) Experimental conditions: $E_i = 2.76$ eV, $\vartheta_i = 45°$, $\vartheta_s = 45°$ and $\varphi_i = 0°$ and $T_S =$ 45 K. The spread in the H atoms' incidence energy δE_i is also shown. Adapted from ref. 361.

The simplest example so far studied with this instrument is that of H scattering from a cryogenic Xe solid surface at an incidence energy of 2.76 eV.[361] Here, classical molecular dynamics simulations performed on a full-dimensional PES constructed from DFT-GGA data perfectly reproduce experimental observations, when using an effective medium theory to fit DFT data.[68] See Fig. 6. This allowed the simulations to be "unpacked", providing more information than one could imagine obtaining from experiment alone.

In fact, it was possible to determine the number of collisions. Here, it is important to recall that a collision is an ambiguous quantity—for example, high impact-parameter collisions that lead to an infinitesimal deflection are, in principle, collisions; but they result in a negligible energy-loss. Using a definition of weak and strong collisions that was based on the distance of closest approach during the trajectory, it was shown that double-bounce trajectories are more important than single-bounce events, even for specular scattering, where one might think single-bounce events would dominate. The tendency of each bounce to direct H atoms out of the plane of detection means that two bounces can compensate out-of-plane momentum such that the trajectory remains in the detection plane. These weak double-bounce events exhibit nearly the same energy loss as that predicted by the single-bounce line-of-centers model.

A large fraction of the observed scattering results from trajectories that visit regions of space below the first layer of Xe atoms (sub-surface multibounce scattering) before returning to the gas phase. See Fig. 7. Overall, these multibounce and subsurface scattering dynamics allow as much as 0.5 eV of the incident 2.76 eV energy to be lost from the H atoms colliding with a solid Xe surface, far exceeding the predicted energy loss of the binary collision model (0.082 eV) normally considered the largest energy loss possible. Subsurface penetration is also responsible for sticking of the H atom, which was computed to occur for 15% of the trajectories.

6.2. H-atom scattering from metals

These studies could be extended to H scattering from Au (111), where electronically adiabatic MD simulations failed dramatically.[353] However, energy loss measurements were in good agreement with classical MD simulations with

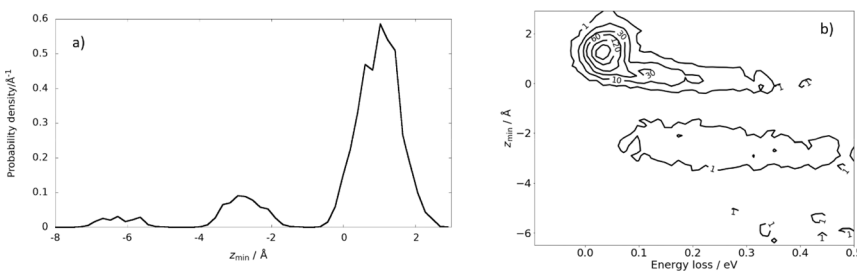

Fig. 7 Subsurface scattering: (a) probability density distribution of the scattering trajectories as a function of distance of closest approach to the surface, z_{min}. The equilibrium positions of the Xe surface atoms define $z_{min} = 0$. (b) Probability correlation distribution comparing the depth of penetration and energy-loss. The numbers on the contour lines indicate the numbers of MD trajectories. $E_i = 2.76$ eV, $\vartheta_i = 45°$, $\vartheta_s = 45°$, and $\varphi_i = 0°$ and $T_S = 45$ K. Adapted from ref. 361.

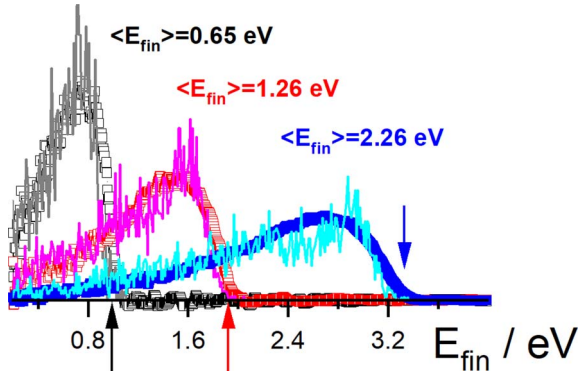

Fig. 8 H scattering from Au(111) at three incidence energies E_{in}. Experimental results (open squares) are compared to theory (solid lines): $E_{in} = 3.33$ eV (blue), 1.92 eV (red), and 0.99 eV (black). Colored arrows mark the three incidence energies. Also shown are the average final translational energies, $\langle E_{fin} \rangle$. The scattering angles are $\vartheta_i = 45°$, $\vartheta_s = 45°$ and $\varphi_i = 0°$ with respect to the [10$\bar{1}$] direction. Adapted from ref. 353 and used with permission under lic. no. 574300005425.

electronic friction applied on a full-dimensional PES.[68] See Fig. 8. Here, Effective Medium Theory (EMT) was fitted to the DFT data[68] and a local density electronic friction approximation was employed.[95,362,363] In the meantime, the EMT formula (originally derived for fcc metals) was derived for bcc metals as well.[67]

The theoretical simulations are thought to provide accurate sticking probabilities, which are difficult to measure experimentally. The theory also reveals a novel sticking mechanism for H atoms, where (as in the Xe case) sub-surface penetration occurs. The electronic friction is so strong in the subsurface region that the H atoms resurface within 100 femtoseconds and thermalize to the most stable binding sites.[353] Similar results were found on six metals[350–352] and on different surface facets,[354] suggesting the generality of the behavior originally seen for Au(111). This allowed a generalization and determination of a quantitative formula for computing the incidence angle and energy-dependent sticking probability of H and D on metals.[351,352] The isotope effect is small[350] and theory could explain this as a compensation effect. Lighter H atoms more effectively excited electron–hole pairs, but D atoms more effectively excited phonons.[364] Theoretical simulations of these scattering experiments were also capable of explaining the isotope effect seen in chemicurrent experiments.[364]

6.3. H-atom scattering from graphene

Advancing in complexity, we next consider the H scattering from graphene. H scattering from graphene grown on Pt was carried out as described above in the discussion of Fig. 8. When grown on Pt, the graphene layer is polycrystalline with two rotational domains and is physisorbed to the metal. The scattering distributions are bimodal with a quasi-elastic component and another that exhibits a large energy loss due to the formation of a transient covalent C–H bond.[360] The transient bond formation channel increases in importance as the incidence angle is scanned from a glancing to a normal direction to the surface, which is evidence that a barrier to forming the C–H bond must be overcome. These dynamics were

investigated from a theoretical perspective using DFT calculations on a free-standing model of the system and fitting with REBO[360] or NN.[365] Classical trajectory calculations also showed bimodal behavior in the energy-loss distributions. Analysis of the trajectories showed that the large energy loss was made possible by the re-hybridization of the C-atom involved in the transient bond, which exerts strong forces on neighboring C-atoms as the delocalized π-bonding network is broken up. In this way, C-atom motion, parallel to the surface, was excited within about 10 femtoseconds, whereas out-of-plane C atom motion was only seen after about 20–30 femtoseconds.

Sticking probabilities (Fig. 9) could be derived from the experiment over a limited range of the normal component of the incidence energy. MD simulations on a full-dimensional PES were in good agreement with those values. Theoretical predictions of the sticking probabilities at higher energies were also made and there is no reason to doubt that they are reliable, although they remain unconfirmed by experiment. RPMD trajectories were run to simulate the ZPE and tunneling, but quantum effects were found to be small. Strictly speaking, RPMD is only valid under thermal conditions and its use in this way is not rigorously correct. To what degree RPMD can be trusted for such applications, would rely on making comparisons to better quantum-dynamics simulations. Very recently, MCTDH calculations on H scattering from graphene with 75 dimensions and using a NN PES have been demonstrated and compared to experiment.[87] These calculations confirmed that quantum effects are small for incidence energies of

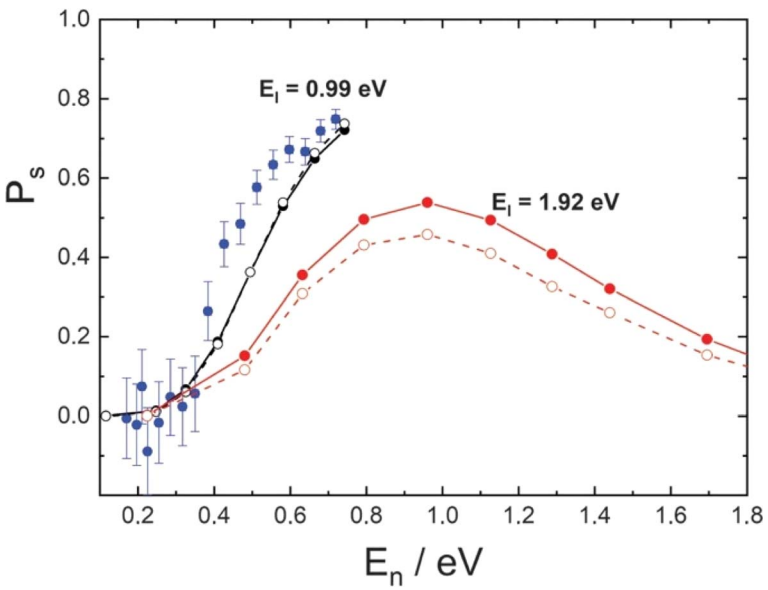

Fig. 9 H-atom sticking probabilities at graphene. Experimentally derived (blue) and theoretically predicted (black) sticking probabilities for $E_i = 0.99$ eV plotted against the normal component of the incidence energy (E_n). Theoretically predicted sticking probabilities for $E_i = 1.92$ eV are shown in red. Theoretical simulations used a full-dimensional EMFT-REBO PES that includes the influence of the Pt substrate with classical molecular dynamics (solid symbols) or ring polymer molecular dynamics (open symbols). Adapted from ref. 360 and used with permission under lic. no. 5743000308890.

1.96 eV, but a marked increase in sticking probability was seen at 0.96 eV incidence energy, due to the influence of quantum effects.

6.4. H-atom scattering from germanium

Most recently, H-atom scattering has been extended to the case of semiconductor surfaces. Again, the interplay between experiment and theory has been crucial. Reminiscent of the H scattering from graphene, for collisions of H-atoms at a Ge (111)-c(2 × 8) surface, a quasi-elastic peak was seen, as well as a channel exhibiting a large energy loss.[357] Interestingly, the threshold of the high-energy-loss channel was coincident with the surface bandgap,[357] suggesting the cause of the bimodal behavior is very different than in the case of graphene. Molecular dynamics simulations were carried out using a high-dimensional NN PES computed with DFT within the Born–Oppenheimer approximation. The calculations matched the quasielastic channel within the uncertainty of the measurements; however, there was no sign of a high-energy-loss channel. This strongly suggested that the high-energy-loss channel does not arise from transient chemical bond formation, but rather is due to promotion of an electron from the valence band to the conduction band. The high-energy-loss channel also increased in importance with increasing translational energy of the H-atom beam, a typical sign of Born-Oppenheimer Approximation failure. The authors concluded that the high-energy H-atom collisions at the surface of the Ge semiconductor were able to efficiently excite electrons from the valence band to the conduction band.[357] The isotope effect was later taken as evidence of a site-specific transition that is related to the electronic structure of the adatoms and rest atoms present on the surface reconstruction.[358]

7. More complex systems for molecule–surface scattering

One of the great successes of gas-phase crossed molecular beams scattering arises from the single-collision conditions afforded by the method. In these experiments, two continuous beams cross one another, each with a density $\rho \sim 10^{11}$ cm^{-3}. The crossing volume of the two beams $V \sim 0.03$ cm^3, as well as the relative velocity $v_{rel} \sim 10^5$ cm s^{-1} and the collision cross-section $\sigma_{coll} \sim 10^{-14}$ cm^2 can be combined in eqn (1) below to calculate the rate of collisions.

$$\frac{d[\text{collision}_{1,2}]}{dt} = \langle \sigma_{coll} v_{rel} \rangle \rho_1 \rho_2 V \quad \left(\sim 3 \times 10^{11} \text{ s}^{-1} \right) \tag{1}$$

When comparing this to the incident flux of one of the beams at the collision zone, 10^{15} s^{-1}, one quickly appreciates that in this experiment, the probability for a single condition is on the order one in a thousand. Hence, the probability that two collisions occur is on the order of one in a million. For reactive processes of complex polyatomic molecules, the single-collision conditions provide an enormous simplification, allowing scientists to observe all of the initially formed reaction products—that is, the results of the first collision—and characterize them quantitatively. See for example ref. 232, 233, 252, 259 and 366.

There is no applicable analogous experiment in surface chemistry, as single-collision conditions are rarely obtained. It is as if we perform a crossed-beams scattering experiment where one beam possesses an atomic density of 10^{22} cm^{-3}. While this simple statement glosses over a great deal, the H-atom scattering from Xe presented above confirms the assertion that it is unlikely that incident atoms and molecules experience a single collision upon encountering a solid or liquid surface.[361] Even more catastrophic to the idea of single-collision surface chemistry is the fact that when a surface reaction is initiated by an incident molecular beam, it is typical that these molecules first adsorb and thermalize with the surface, possibly while also dissociating to form the first reaction intermediates. Products are then formed only after these intermediates diffuse—possibly, they may also isomerize—and react to final products. Often this involves reaction with other pre-adsorbed molecules. Another key difference is that—unlike the pristine homogeneity of a vacuum—surfaces are heterogeneous. Hence, diffusion of intermediates to especially reactive sites of the surface is often essential to the mechanism. This is even true when carrying out experiments with nearly perfect single-crystal surfaces.

Despite these critical differences, experimental methods for reactive scattering on surfaces using molecular beams have advanced dramatically in recent years. The usefulness of molecular beams for reactive scattering at surfaces can be seen in the recently obtained results using the "isothermal pulsed molecular beams" method.[367,368] In this approach, molecular beams deposit reactants at a catalytic surface within the well-controlled conditions of an ultra-high-vacuum chamber. Desorbing products are then detected by electron bombardment ionization quadrupole mass spectrometry. Adsorbates are simultaneously detected using infrared absorption spectroscopy (IRAS). An apparatus for applying this method has been described.[369] This approach has quite important advantages over the well-known temperature programmed reaction (TPR) method, where reactants are deposited at low temperature and desorbing products are detected while a linear temperature ramp is applied to the surface. Most importantly, the reactions important to the catalysis can be studied at controlled and variable temperatures in an isothermal experiment.

This method has been applied to answer a variety of interesting questions in catalysis. Surface accessibility of subsurface hydrogen in palladium nanoparticles was investigated, and it was shown that diffusion between the surface and bulk is strongly altered by C atoms that can bind near low-valence step-edges.[370] In other work, hydrogen recombination[371] as well as reaction of hydrogen with adsorbed 2-butene[372] was found to involve subsurface hydrogen. The "spectator effect", which is closely related to ligand-directed hydrogenation,[373] was studied in selective partial hydrogenation of acrolein.[374,375] Here, the influence of surface crowding by nonreactive molecules could be shown to have a profound impact on the chemistry. In another study, it could be shown that the adsorption of butanal is accompanied by keto–enol isomerization to form three adsorbed intermediates,[376,377] whose chemistry controls the product formation.

Also using this method, methanol oxidation to methyl formate was observed on Au (332).[378–380] Nanoporous gold is an important catalyst for this reaction—its high surface area and the ability of Ag impurities in this material to activate oxygen are crucial.[381] Despite the many potential differences to the nanoporous catalyst, very similar reactivity was observed on single-crystal Au (111) and (332).

For these pure gold catalysts, the oxygen was introduced as gas-phase atoms from an effusive molecular beam. The experiments clearly showed the efficient formation of the desired methylformate product and, using IRAS, the buildup of adsorbed bidentate formate, which slowly poisoned the catalyst. Due to the well-controlled conditions of these experiments, insights into the reaction mechanism could be obtained. A previously proposed mechanism for methylformate formation involving recombination of two adsorbed methoxy intermediates[382,383] could be confirmed. Over-oxidation of the methylformate to undesired side products was also seen and conditions could be found where it could be suppressed. A special adsorbed oxygen species was inferred that is capable of oxidizing methylformate.[380]

7.1. Kinetics of reactions at surfaces

These experiments give a glimpse of the power of reactive molecular beam scattering in surface chemistry, a power that can be amplified when combined with quantitative measurements of reaction rates. Such experiments were first developed in the early 1970's, with the advent of the molecular beam relaxation spectroscopy.[384,385] This method employed a modulated molecular beam to dose the surface and an electron bombardment ionization mass spectrometer to detect products. The temperature-dependent phase shift could be used to gain information on the reaction kinetics. In one of the successes of this technique, it could be seen that CO oxidation on a stepped platinum surface proceeds *via* a Langmuir–Hinshelwood and not an Eley–Rideal mechanism.[386]

More recently, a family of related techniques have become possible that take advantage of modern pulsed molecular beams and pulsed lasers as well as ion imaging. The velocity-resolved kinetics (VRK) methods[387–389] now make the experimental determination of reaction rates much more quantitative. Discovered serendipitously while performing state-to-state time-of-flight measurements involving molecular beams scattering from Pt,[390] VRK relies on laser methods that simultaneously obtain the densities and velocities of molecules, allowing accurate determinations of molecular flux. To appreciate this point, consider the units involved in the simple desorption reaction expressed by the following kinetic eqn (2):

$$\frac{\mathrm{d}[\mathrm{CO}]_{\mathrm{g}}}{\mathrm{d}t} = -\frac{\mathrm{d}[\mathrm{CO}]_{\mathrm{sur}}}{\mathrm{d}t} = k_{\mathrm{des}}[\mathrm{CO}]_{\mathrm{sur}} \quad (2)$$

Because the concentration of CO at the surface $[\mathrm{CO}]_{\mathrm{sur}}$ is in units of surface density and because k_{des} is a 1st-order rate constant with units of inverse time, the rate of production of gas-phase CO has units of flux. Hence, monitoring the reaction rate *via* detection of gas-phase CO requires methods to measure flux, which as just mentioned may be accomplished *via* a simultaneous measurement of density and velocity. An additional advantage of measuring molecular velocities arises as it becomes possible to accurately calculate when the molecule left the surface on its way toward the detection laser beam. Hence, by using short pulsed molecular beams to initiate the reaction, the reaction time at the surface can be determined with less than ~10 μs uncertainty.

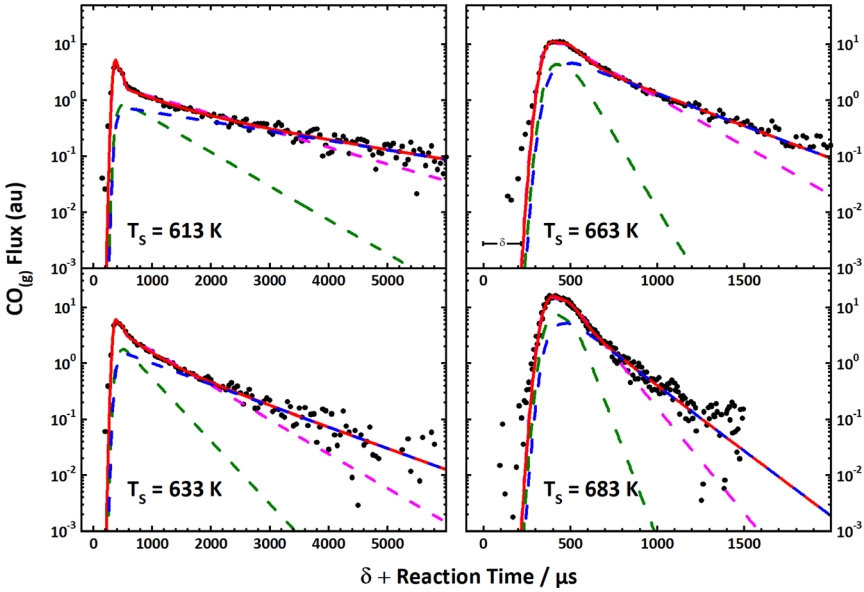

Fig. 10 The first velocity-resolved kinetic data. In this experiment, a short-pulsed CO molecular beam was incident at a Pt (111) surface at time δ, determined in a separate experiment. The CO molecules leaving the surface were excited to the metastable $\tilde{a}^3\Pi$ state <1 mm away from the surface. The metastable molecules were subsequently ionized ~12 mm from the surface using 1 + 1 REMPI *via* the $\tilde{b}^3\Sigma^+$ state. The delay between the two laser pulses was fixed, defining the velocity of the molecules being detected. The timing of the pulsed molecular beam was then varied with respect to both laser pulses to observe the residence time of the molecules on the surface. Bi-exponential kinetics (solid black circles) can be clearly seen. The two components are related to (1) desorption from terrace sites (green dashed line) and (2) diffusion from steps to terraces followed by desorption (magenta dashed line). The sum of the two components (blue dashed line) matches the data well. Note the vertical axes are logarithmic. Adapted from ref. 390.

These simple insights, along with the remarkably high signal-to-noise ratio afforded by VRK, permitted the first bi-exponential desorption traces to be observed,[390] from which the role of terraces and steps could be discerned. See Fig. 10. Here, a rather cumbersome two-laser scheme was employed that relied on a detailed knowledge of the spectroscopy of CO.

This approach to the kinetics of surface reactions was made more general by employing non-resonant multiphoton ionization (MPI) in concert with slice ion imaging.[124] Here, non-resonant MPI was performed by focusing the output of a titanium–sapphire laser—available with ~1 mJ pulse energies and a 35 fs pulse duration operating at a 1000 kHz repetition rate. This allows experiments with many molecules not normally considered suitable for laser detection. For example, both H_2O[391] and CO_2 [387] products from H_2 and CO oxidation on Pt, respectively, could be studied with VRK, as could formic acid (HCOOH),[392] NH_3,[393] H_2,[394,395] CO[387] and NO.[396] Detection of many other molecules is also possible with this method.

Accurate desorption rate constants obtained using VRK contain valuable information on molecule–surface interactions, adsorbate binding energies and

diffusion barriers, which can be derived using transition-state theory (TST). For example, NO desorption rate constants from Pd(111) and (332) provided accurate NO binding energies (1.766 ± 0.024 eV) and diffusion barriers (0.29 ± 0.11 eV).[396] Similar results were obtained from VRK measurements of NH_3 desorption from Pt(111) and (332). Here, the NH_3 binding energy to Pt(111) (1.13 ± 0.02 eV) and the diffusion barrier (0.71 ± 0.04 eV) could be accurately derived. In addition, NH_3's binding-energy preference for steps over terraces on Pt (0.23 ± 0.03 eV) was obtained. The influence of co-adsorbed oxygen on the NH_3-binding energy—it increases by 0.15 eV—and diffusion barrier—it increases by 0.39 eV—was also found.[397] Formic acid desorption rates measured with VRK also yielded an accurate desorption energy (0.639 ± 0.008 eV) from Pd(111) as well as the diffusion barrier (0.37 ± 0.13 eV) across 111 terraces. In other VRK measurements of the recombinative desorption rates of hydrogen from Pd, the dissociative adsorption energy of H_2 and its isotopic variants to Pd were obtained. In fact, the kinetic data were even sensitive to hydrogen diffusion between the surface and the bulk; hence, the bulk absorption energy could also be obtained.[394] Where comparison is possible, the binding energies obtained above compare well with results from single-crystal adsorption micro-calorimetry.[398,399]

One advantage of VRK (or for that matter any accurate desorption kinetics measurement) is that, in addition to binding energies, accurate diffusion barriers can be derived. This is because a TST rate constant has both an energetic term—the energy needed to reach the transition state—and an entropic term, which mainly influence the pre-factor. The experiment provides information on both and since the entropy of the adsorbate is strongly influenced by its propensity to diffuse, desorption rate constants also reflect the barriers to diffusion. The three examples above are instructive in several ways. For example, the ratio of the diffusion barrier to desorption energy in all three was much larger than the commonly used 12% rule.[400] For ammonia in particular, accurate binding energies and diffusion barriers have significant implications for engineering models of the Ostwald process, where ammonia is oxidized to NO. Specifically, it was possible to understand why established rate models of the Ostwald process incorrectly predict low selectivity and yields of NO under typical reactor operating conditions. These errors are likely due to a failure of the assumption of mean-field kinetics, used in those models.[393]

Perhaps the most important impact of VRK stems from its high accuracy and precision. The accuracy of the rate constants derived from VRK could be demonstrated using the principle of detailed balance. When desorption rate-constants were directly computed from sticking probabilities and other experimentally available quantities and compared to VRK rates, agreement was within the signal-to-noise of the VRK experiments—see Fig. 11.[395] Note that this required no adjustable parameters. This not only provides a striking example of the power of the principle of detailed balance, it also reveals the strengths and weaknesses of commonly applied approximations used in TST for surface reactions. This work helped show that for this reaction, quantum effects are large even at high temperature. Beyond zero-point energy effects, which are well known, the wave nature of the light adsorbed atom produces a quantum delocalization and concomitant high entropy that dramatically reduces its recombination rate constant.[395] The H-atom's spin degeneracy also contributes a factor of four

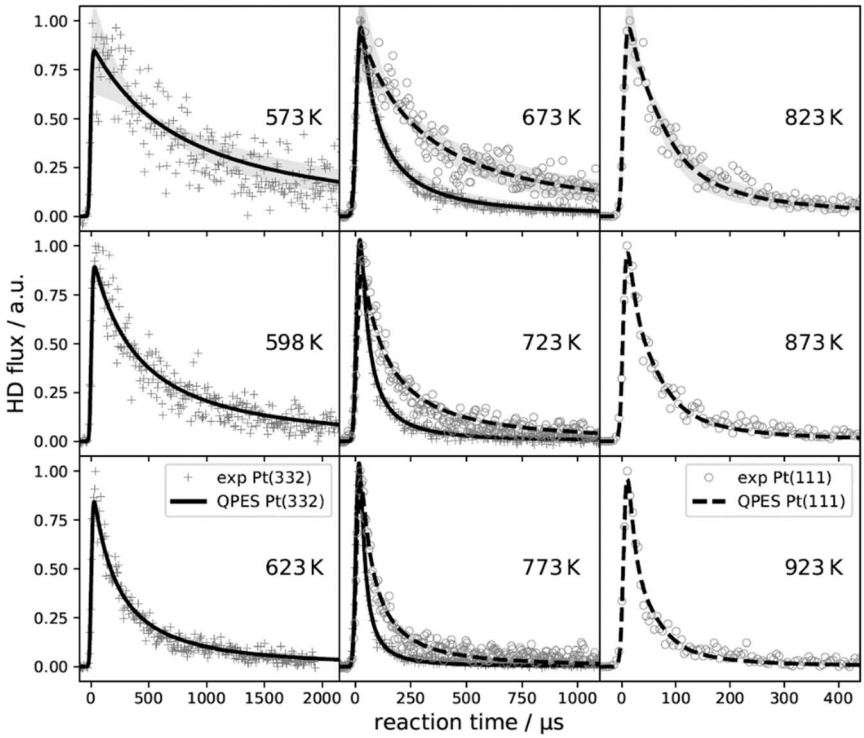

Fig. 11 Velocity resolved kinetics (VRK) of hydrogen atom recombination on Pt (111) and Pt (332). Measured reaction rates for Pt (111) (∘) and Pt (332) (+) are compared to the results of a quantum rate model based on the principle of detailed balance and experimentally derived dissociative sticking coefficients (dashed and solid lines). The temperature dependence and the transient rate of the measurements is quantitatively captured by the quantum rate model for both facets. The shaded regions of the top three panels indicate the 2σ-uncertainty. Excellent agreement was achieved without adjustable parameters. Adapted from ref. 395 and used with permission under lic. no. 5743000493441.

reduction in the rate, as combining H atoms to form the ground electronic state of H_2 is only possible for one of the four spin combinations.

The high accuracy demonstrated for VRK provides some of the first experimentally derived thermal rate constants that are accurate enough to provide benchmarks for first-principles rate theories for surface chemistry. The VRK benchmarks were exploited in a recent theoretical study. Using a 6D PES generated with machine learning from DFT data obtained at the GGA level, Ring Polymer Molecular Dynamics (RPMD) was used to directly obtain thermal rate constants.[88] The derived rate constants, which exhibited large quantum effects, were (only) a factor of two lower than those from experiment when the PBEα-vdW-DF2 functional was used.

Surface site-specific rate constants for reactive processes like CO oxidation on Pt can also be obtained with VRK.[387] These experiments revealed another advantage of measuring product velocity—when reactions occur *via* different mechanisms, they may lead to products with different speed distributions—see Fig. 12. In this case, CO oxidation at terraces produced hyperthermal speed

distributions of CO_2, whereas the dominant reaction occurring at steps led to CO_2 products with thermal speed distributions. Subsequent theoretical calculations showed that CO_2 is bound more strongly at steps than at terraces, due to charge transfer forming a bent CO_2^--like adsorbate.[401]

Combining kinetic data with product velocity distributions can provide additional information on a surface reaction's energy landscape, as was shown in a VRK study of the decomposition of formic acid to CO_2 on Pt (111). Here, the rate limiting reaction is decomposition of the bidentate formate intermediately formed after O–H bond dissociation at the Pt surface.

$$HCO^*O^* \rightarrow H^* + CO_{2(g)} \quad (3)$$

The asterisks in the chemical eqn (3) indicate the atoms bound to the metal in the formate intermediate. Temperature-dependent VRK data was analyzed to obtain the forward reaction's activation energy, which was taken as a measure of the barrier to the forward reaction, while the maximum measured CO_2 translational energy was taken as a measure of the barrier height for the reverse reaction.[402] The difference between these two barrier heights gave an independent

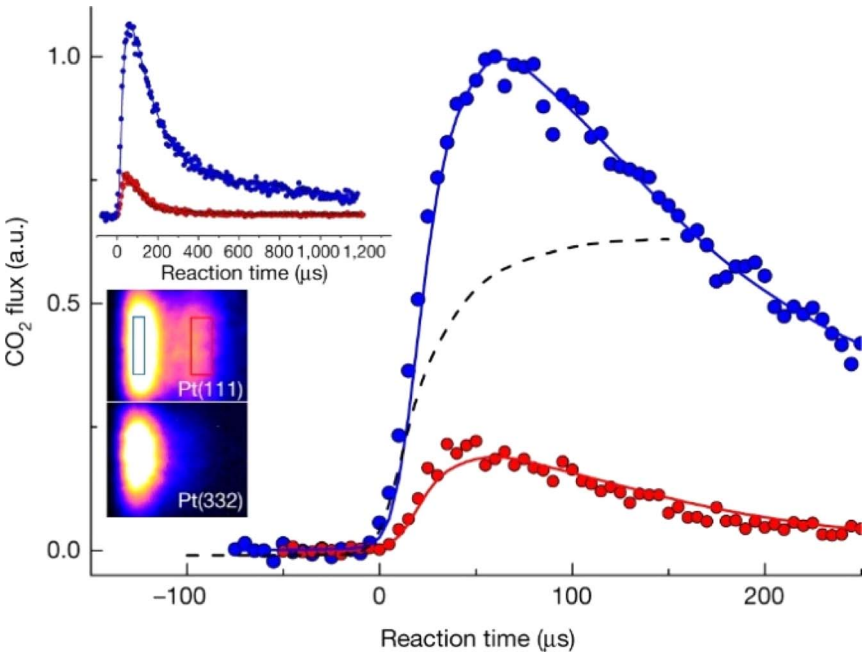

Fig. 12 Velocity-resolved kinetics of CO_2 from CO oxidation at a Pt surface. The lower left inset shows an ion image with velocity-space integration windows for a hyperthermal (red rectangle; 1280–1610 m s^{-1}) and a thermal (blue rectangle; 420–590 m s^{-1}) channel. The kinetics of the two velocity groups are shown as blue and red circles in the upper inset and in the main figure. The thermal velocity products result from reaction at steps, whereas the hyperthermal velocities arise from reaction at terraces; note that the hyperthermal channel is visible for the (111) surface only. The solid red and blue lines are fits using a kinetic model involving two reactions at steps and one at terraces. The dashed black line represents the measured CO dosing function. The surface temperature was 593 K. Adapted from ref. 387.

measure of the heat of formation of the bidentate formate bound to Pt (111), which was in good agreement with single-crystal adsorption calorimetry.[403] This procedure could be repeated as a function of oxygen surface coverage on both Pt (111) and (332), providing information on the reaction pathway. While this investigation made measurements of the decomposition of formate, from the derived energy diagrams it was also possible to conclude what a Pt catalyst requires for optimal functionalization of CO_2 with hydrogen. The results of this work clearly showed that CO_2 could be most easily activated to a formate adsorbate on a Pt surface with a high defect density and oxygen-lean or oxygen-free conditions.

Perhaps of greatest future significance, VRK of surface reactions can be used to identify reaction intermediates, providing critical information on reaction mechanisms in catalysis (**https://doi.org/10.1039/D3FD00174A**). In another paper appearing in this *Faraday Discussion*, formic acid decomposition on palladium exhibited a "fast" and a "slow" kinetic channel for CO_2 production. These channels are well-resolved—see Fig. 13—by VRK and the branching between them is easily measured and, moreover, strongly dependent upon isotopic substitution (**https://doi.org/10.1039/D3FD00174A**). Here, theoretical examination of measured kinetic isotope effects makes it possible to assign the fast and slow channels to decomposition of two reaction intermediates—carboxyl and bidentate formate, respectively.

Since these studies were reported, additional variants of VRK have been reported. A high-repetition-rate version of VRK drastically reduces measurement time and may be useful for following nonstationary catalysts, for example, undergoing poisoning or activation.[388] Laser-induced desorption VRK provides possibilities to directly detect reaction intermediates. Here, a femtosecond pulse

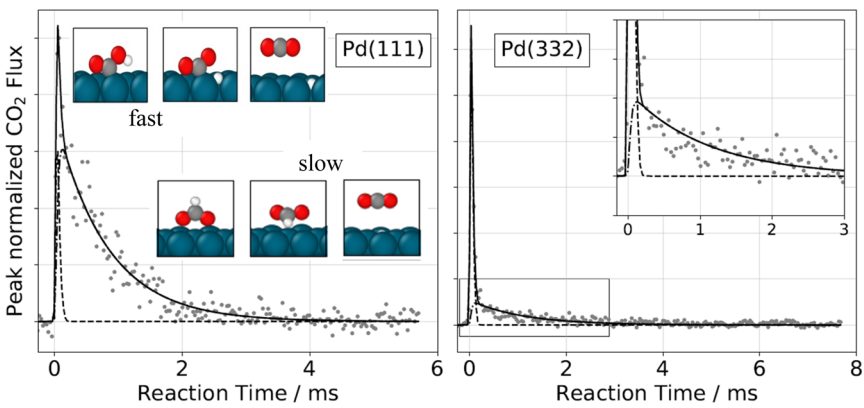

Fig. 13 Observation of two temporally resolved CO_2 formation channels in formic acid decomposition on Pd. Typical peak-normalized kinetic traces of CO_2 on Pd(111) (left) and Pd(332) (right) at 403 K using HCOOH. The solid lines are a kinetic fit (see https://doi.org/10.1039/D3FD00174A). The inset in the right panel shows an enlarged view of the slow component, which decays over several milliseconds at this temperature, whereas the fast component exhibits a time dependence similar to that of the incident pulsed molecular beam (dashed line). The insets in the left panel show the reactant, transition state, and product structures computed from DFT for the fast and slow channels on Pd(111).

of laser light is used to desorb reaction intermediates *via* a DIMET (desorption induced by multiple electronic transitions) process. These hyperthermal desorbates are then detected in the gas phase *via* laser ionization.[389]

7.2. Hot beams

An important opportunity for both gas-phase and gas–surface experiments has been pursued by Minton and others through the development of hyperthermal sources of atomic species like O, N, F, and Ar using a laser detonation source.[159] This source can produce translational energies in the several-eV range that are important in upper atmospheric chemistry and space science. It has been demonstrated for O atoms that only the electronic ground state has significant population in these sources, which makes it possible to study reactive collisions involving high barriers and endothermic processes with the reaction dynamics theories described earlier. This has been demonstrated both for crossed-beams studies, such as for the O + H_2 reaction,[404] and for beam-surface experiments, such as O + graphite[147,345] and O + ionic liquids.[405] Recent gas-phase reactions have focused on reactions that are important in hypersonics, including N + O_2 (ref. 406) and O + NO,[407] where it is possible to use the results to validate reaction dynamics calculations with high-quality PESs, and then the calculations can be used to generate rate coefficients that are crucial for atmospheric modelers. The gas–surface hyperthermal beam studies have also been used to provide insights about the structure of ionic-liquid interfaces,[408,409] and about processes that are important for degradation of hypersonic and space vehicle components.[410,411]

7.3. Molecular scattering from liquid surfaces

The scattering of atoms and molecules from liquid surfaces became popular after the advent of the scraped rotating-wheel method, originally developed by Fenn to measure evaporation rates from liquid surfaces.[412] Here, a molecular beam is incident upon a low-vapor-pressure liquid that forms a film on a rotating disk within a vacuum chamber. A metal or Teflon scraper ensures that the surface remains clean. Scattered molecules are detected under collision-free conditions; hence, the observations reflect the fundamental interactions experienced by the molecule at the vacuum–liquid interface. Pioneering work from the labs of Gil Nathanson[413,414] used neutral time-of-flight (TOF) mass spectrometry to obtain velocity and angular distributions of scattered molecules.[413,414] Other labs have since employed laser-based methods including LIF,[415] infrared[416] and UV-vis[417] absorption spectroscopy. Two excellent reviews appeared in 2016,[86,347] outlining many of the common observations seen in this field. Initially, inelastic scattering was the focus of the field; here, two channels—trapping followed by desorption as well as direct inelastic scattering—are often seen. This is not only true for inert systems like rare-gas atom scattering from liquid surfaces, but also for radical scattering.[418]

More recently, attention has turned to reactions of incident atoms and molecules at liquid surfaces. This has proven useful, for example, to gain an understanding of the structure of liquid surfaces, an idea that has been demonstrated for pure molecular liquids, for salty solutions, and especially for ionic liquids. For example, Al atom beams could probe the surface content of fluorine in ionic liquids through a reaction forming hyper-thermal AlF, which could be detected by

LIF.[419] Similar ideas were exploited for OH reactive scattering from ionic liquids, where the surface structure of several ionic liquids was found to be independent of the ionic head group and rather dominated by the alkane side chain.[420] Reactions of solvated electrons initiated by Na atom adsorption at a glycerol surface were also reported.[421]

The cylindrical, liquid micro-jet of Faubel, Schlemmer and Toennies[422] is an innovation that has raised the ambitions of this field and, since its invention, efforts have intensified to study the vacuum/water interface. For example, with the ability to introduce liquid water into a vacuum chamber, photoelectron spectroscopy became possible, for example using core-level photoelectron spectroscopy[423] to measure work functions of liquid-water surfaces.[424]

However, methods for scattering molecules from surfaces of high-vapor-pressure liquids like water are not yet fully mature. A recent review discusses many of the "lessons learned" in developing liquid microjets for scattering experiments.[346] Here, an important potential pitfall must be attended to; rapid evaporation from the surface of liquid microjets is a stark reality of introducing a high-vapor-pressure liquid to a vacuum. There is a danger that molecules scattered from the surface of liquid water may be re-scattered by gas-phase water molecules evaporating from the jet. The evaporation rate depends on the radius of the cylindrical microjet; the smaller the radius, the less dense the vapor sheath around the liquid.[347] Salts and/or surfactants may also be introduced to further lower the vapor pressure of the liquid. In addition, water evaporation is strong enough that the liquid's temperature drops with distance from the nozzle, an effect that of course also lowers the evaporation rate. The temperature of the liquid can be determined from the velocity distribution of evaporating Ar that has been pre-dissolved in the water. This distribution is then fitted to a Maxwell–Boltzmann function and a temperature is obtained. Of course, this relies on an assumption that the sticking probability of Ar to cold liquid-water surfaces is velocity-independent.

While the technical challenges are formidable, the future appears promising, especially for reactive scattering from aqueous surfaces. Reactions of solvated electrons at a water interface (similar to those described above for glycerol) have been demonstrated.[425] Uptake of gas-phase molecules has also been studied by comparing scattering from the glass nozzle to that from the aqueous surface. It could be shown, for example, that HCl is efficiently taken up by the solution and experiments with DCl showed no isotope exchange, strongly suggesting that only the molecules that undergo direct inelastic scattering fail to dissolve.[426] In another example of the potential of this approach, Br_2 was found to emerge back to the gas phase after a beam of N_2O_5 collided with an aqueous microjet with a large concentration of dissolved LiBr.[427] These experiments reflect chemistry thought to be important in sea-water aerosol droplets.

One specific problem with cylindrical microjets that may ultimately limit their usefulness is their small size—they are typically on the order of 30 μm in diameter. Direct comparison of scattering signals from rotating-wheel and cylindrical-microjet geometries shows at least a two-order of magnitude loss of scattering signal when using the microjet.[429] It would, of course, be a tremendous practical advantage to develop flat liquid jets. In fact, it has been known since the 1960's that colliding cylindrical jets of water form flat leaf-like structures, which may be many mm in size—see Fig. 14.[428]

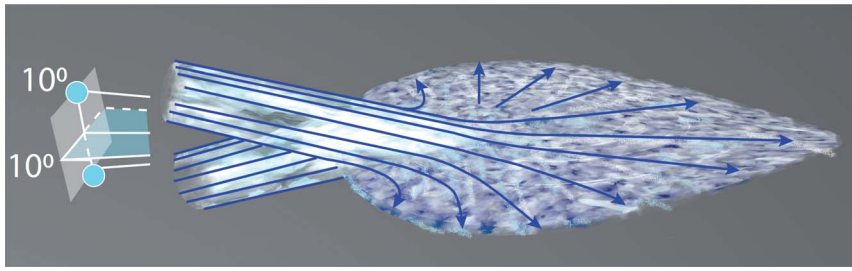

Fig. 14 Planar sheets of water are formed by collisions of cylindrical jets. Such leaf-like structures can be many mm in extent. This is an original figure based on a figure from ref. 428.

Inspired by this, molecular beam scattering from flat liquid jets has been recently achieved for dodecane,[430,431] which has a vapor pressure about 1% that of water. Extending these successes to aqueous interfaces will doubtless still be challenging, in particular because the flat-jet geometry is markedly less favorable for the formation of a gas-sheath than is the cylindrical jet. Furthermore, flat jets exhibit temperature gradients;[432] however, this does not appear to be an insurmountable problem. There is every reason to believe that this approach will bear fruit in the near future.

8. Perspectives

The purpose of this review has been to present highlights of recent work using molecular scattering for the study of basic chemical reactivity in the gas phase and at surfaces. We have emphasized emerging laboratory methods that allow new types of measurements to be made and the fruitful cooperation between experiment and theory. In this final section, we claim an ability to see the future and point out new directions that we deem to be especially ripe for study. Unfortunately, this section may read like a laundry list of half-baked research proposals, which it is. Nevertheless, we hope that it may still provide value by inspiring readers to think more deeply along certain lines that lead them to concrete new work.

The study of nonadiabatic processes is becoming more and more common in both gas-phase and gas–surface collision processes, with a broader and broader range of processes being considered, including species that are generated in highly excited states and that have many possible product channels and electronic states. At the most fundamental level, full quantum calculations are performed. These are primarily restricted to gas-phase processes, but provide valuable insight concerning quantum interference, including the geometric phase effect, and concerning spin-forbidden processes that can sometimes be crucial, even if they are rare. Trajectory surface hopping is gradually becoming available in public-domain codes (along with the ability to calculate nonadiabatic couplings), and has already proven important in studying a variety of gas-phase and gas–surface processes. It will be important to carry out further theory development in this field, as well as to extend the range of problems that can be studied.

For experimental crossed molecular beams scattering studies, the development of new atomic and molecular beams and detection methods is essential. Development of high-quality atomic and molecular beams, especially highly intense beams with narrow velocity spread, are important in the study of reactive-scattering experiments. This allows us to measure detailed differential cross sections for reaction products at specific quantum states, providing most thorough dynamics information for a specific chemical reaction. New laser photolysis techniques and other methods, such as discharge and thermal dissociation, *etc.*, can be applied to generate high-quality atomic and radical beams for future crossed-beams scattering studies.

In addition to new atomic and molecular beams, development of low-background, more universal and highly sensitive detection methods are certainly desirable. For neutral reactive-scattering experiments, an efficient ionization detection scheme is the key. Therefore, a better ionization scheme, especially efficient soft VUV ionization, is important for further development of crossed-beams methods. One promising direction is the VUV ionization detection based on free electron laser (FEL) light sources, such as the Dalian Coherent Light Source, which can provide intense VUV laser light. Direct VUV FEL ionization can provide universal and efficient detection schemes for atomic and molecular species. Higher-repetition VUV FELs, which are based on superconducting accelerator technology, will certainly become a more powerful tool for universal detection of reactive-scattering products for complex chemical reactions.

More powerful and accurate quantum-dynamics calculation methods will be further developed; thus, the dynamics of more complex reactions can be investigated accurately, especially when accurate potential energy surfaces for complex reactions become available. This will enable us to acquire more accurate dynamics and kinetics information for both elementary and complex chemical reactions. Further development of dynamics theory, in concert with the development of advanced crossed-beams scattering experimental methods, will surely drive the field of chemical reaction dynamics to become a more exact science. Looking to the future, accurate calculations and predictions of both dynamics and kinetics for all chemical reactions may soon be a reality, with the help of AI technologies.

For gas–surface dynamics, there has been an explosion of interest in adding friction-based methods to incorporate energy transfer involving degrees of freedom that are not explicitly included in the dynamics. We expect this to continue, such that friction will become a standard feature in dynamics calculations, enabling the connection between dynamics and reaction-kinetics studies.

The field of cold collisions also provides new vistas for exploring quantum phenomena. Although the possibility that reactive bimolecular collisions at very low temperatures might access the regime where Wigner tunneling might be important, which was appreciated long ago and calculations using quantum scattering have been available for some time,[433] experimental studies within this regime have primarily been a recent phenomenon due to interest in Bose-Einstein condensates involving diatomic molecules, and in interstellar kinetics. This will stimulate further work, both experiment and theory, to explore the consequences of reactions in this regime. We also note the attractive possibilities of using ions

in cold collisions, for example creating cold plasma by combining negative and positive ions.

Growing interest in hypersonic flight and in vehicle reentry from lunar missions and beyond will continue to stimulate interest in future studies of hyperthermal reaction dynamics. This regime can be effectively studied using quasi-classical trajectory methods, but with significant challenges in the treatment of multiple electronic states and their couplings.[406]

The future of surface chemistry involves understanding reaction mechanisms under the high temperature and pressure conditions where real catalysis takes place; both theoretical and experimental reaction kinetics will be essential (**https://doi.org/10.1039/D3FD00174A**). Micro-kinetic modeling forms the underlying mathematical framework of catalysis, and to establish a fundamental foundation, existing rate theories must be improved[395] and new ones must be developed. The aim is to accurately predict reaction rates from theory. Comparison of experiment and theory at the level of elementary reaction rates is an activity that is rarely undertaken.[88] Much more of this will be needed in the future. Experimental methods for following the kinetics of reactions have been improving, but we will also need methods to follow the time-dependent concentrations of reaction intermediates. This calls for new means for sensitive and specific, yet universal, detection of adsorbates. Laser-induced desorption followed by gas-phase ionization[389] has the potential to provide mass-spectrometric-like signatures of intermediates, if it can be combined with a universal means of detection (*e.g.*, electron bombardment ionization or soft VUV ionization). Multi-mass imaging[130] and covariance imaging[129] are two other excellent experimental methods that are likely to find application in problems of reactive scattering from surfaces.

Real catalytic conditions give rise to dynamic changes in structures at the interface[434] that may produce transient reactive configurations. Identifying these reactive configurations is one of the most important goals for future work. Time-resolved microscopies and other experimental methods promise such observations, but it remains highly challenging to link observations of reacting systems under real conditions to fundamental quantities that might allow non-empirical models to be developed. This is where theoretical discovery of reaction mechanisms in surface chemistry may become much more important. The structure of such "theoretical discovery" of mechanisms has already been demonstrated for gas-phase reactions.[435,436] It is reasonable to forecast that such methods will be automated[437] and enhanced with machine-learning algorithms and eventually become useful for surface chemistry and heterogeneous catalysis.

Machine learning has great potential for future creative applications; we believe we have so far just seen the tip of the iceberg. For example, it has recently been shown that electronic Hamiltonian matrices can be machine learned.[438] This holds out the possibility that machine learning could lead to predictive models, or at least be much more transferable between related systems.

Quantum dynamics is another frontier; while, especially for surface chemistry, it is rarely used, here, we acknowledge its common *ad hoc* use when it is incorporated into transition-state theory. High-dimensional calculations have recently been demonstrated with 75 nuclear degrees of freedom using MCTDH methods.[87] Future application of these methods will lead to a deeper understanding of

tunneling and reaction resonances as well as the influence of nuclear and electron exchange symmetry on surface chemistry.[395]

The molecular-scattering methods reviewed in this paper have proven to be extremely useful in revealing the basic principles of gas-phase chemistry, surface chemistry and even reactivity in liquids. The major opportunity afforded by these methods, which is not as easily exploited in other types of experiments, is that it can be combined with first-principles theory and in so doing, much deeper insight becomes possible. The major reason for this arises from the fact that molecular-scattering experiments deliver many qualitative and especially quantitative observables. These include not only the elementary reaction products' identity, but also their quantitative scattering properties like recoil angle, speed and quantum-state population distributions. This large diversity of accurately determined observations places extreme pressure on theory to come up with the right answers for the right reasons. Once this high standard has been reached, the theory may be unpacked to learn aspects of reactivity that cannot be directly seen in the laboratory. New directions in molecular scattering exploit the fruitful collaboration of experiment and theory using the improving tools developed by experimentalists and theorists. While it is unlikely that we will ever reach a point where everything can be computed from theory, we see an extremely bright future, where few problems remain intractable, when the creative spirit is applied to, on the one hand, develop and perfect new measurement methods that make new observations and, on the other, exploit the advance of computational science to explain them.

Conflicts of interest

There are no conflicts of Interest amongst the authors.

Acknowledgements

GCS was supported by ONR MURI Award N00014-22-1-2661. Open Access funding provided by the Max Planck Society.

References

1 M. Born, W. Heisenberg and P. Jordan, *Z. Phys.*, 1926, **35**, 557–615.
2 P. A. M. Dirac, *Proc. R. Soc. London, Ser. A*, 1929, **123**, 714–733.
3 M. Born and R. Oppenheimer, *Ann. Phys.*, 1927, **389**, 457–484.
4 H. Eyring and M. Polanyi, *Z. Phys. Chem.*, 1931, **12**, 279–311.
5 H. Eyring and M. Polanyi, *Z. Phys. Chem.*, 2013, **227**, 1221–1245.
6 H. Eyring, *J. Chem. Phys.*, 1935, **3**, 107–115.
7 H. Eyring, *Trans. Faraday Soc.*, 1938, **34**, 0041–0048.
8 F. T. Wall, L. A. Hiller and J. Mazur, *J. Chem. Phys.*, 1958, **29**, 255–263.
9 N. Basco and R. G. W. Norrish, *Can. J. Chem.*, 1960, **38**, 1769–1779.
10 A. B. Meinel, *Astrophys. J.*, 1950, **111**, 555.
11 J. D. McKinley, D. Garvin and M. J. Boudart, *J. Chem. Phys.*, 1955, **23**, 784–786.
12 A. L. Schawlow and C. H. Townes, *Phys. Rev.*, 1958, **112**, 1940–1949.
13 T. H. Maiman, *Nature*, 1960, **187**, 493–494.
14 J. V. V. Kasper and G. C. Pimentel, *Phys. Rev. Lett.*, 1965, **14**, 352.

15 R. N. Zare, *Annu. Rev. Anal. Chem.*, 2012, **5**, 1–14.
16 L. O. Hocker, M. A. Kovacs, C. K. Rhodes, G. W. Flynn and A. Javan, *Phys. Rev. Lett.*, 1966, **17**, 233.
17 J. T. Yardley and C. B. Moore, *J. Chem. Phys.*, 1966, **45**, 1066.
18 A. M. Ronn, *J. Chem. Phys.*, 1968, **48**, 511.
19 W. J. Tango, J. K. Link and R. N. Zare, *J. Chem. Phys.*, 1968, **49**, 4264.
20 K. Sakurai and H. P. Broida, *J. Chem. Phys.*, 1969, **50**, 2404.
21 F. P. Schäfer, W. Schmidt and J. Volze, *Appl. Phys. Lett.*, 1966, **9**, 306–309.
22 P. P. Sorokin, J. R. Lankard, E. C. Hammond and V. L. Moruzzi, *IBM J. Res. Dev.*, 1967, **11**, 130–148.
23 J. C. Polanyi, *Acc. Chem. Res.*, 1972, **5**, 161.
24 J. C. Polanyi, *Angew. Chem., Int. Ed.*, 1987, **26**, 952–971.
25 E. H. Taylor and S. Datz, *J. Chem. Phys.*, 1955, **23**, 1711–1718.
26 D. Herschbach, G. H. Kwei and J. A. Norris, *J. Chem. Phys.*, 1961, **34**, 1842.
27 Z. Herman, J. D. Kerstetter, T. L. Rose and R. Wolfgang, *J. Chem. Phys.*, 1967, **46**, 2844.
28 W. R. Gentry, E. A. Gislason, Y. T. Lee, B. H. Mahan and C. W. Tsao, *Discuss. Faraday Soc.*, 1967, **137**, 137–145.
29 Y. T. Lee, J. D. McDonald, P. R. Lebreton and D. R. Herschbach, *Rev. Sci. Instrum.*, 1969, **40**, 1402.
30 Y. T. Lee, *Angew. Chem., Int. Ed.*, 1987, **26**, 939–951.
31 C. C. J. Roothaan, *Rev. Mod. Phys.*, 1951, **23**, 69–89.
32 N. C. Blais and D. L. Bunker, *J. Chem. Phys.*, 1962, **37**, 2713.
33 M. Karplus, R. D. Sharma and R. N. Porter, *J. Chem. Phys.*, 1964, **40**, 2033.
34 D. G. Truhlar and A. Kuppermann, *J. Chem. Phys.*, 1970, **52**, 3841.
35 A. Kuppermann and G. C. Schatz, *J. Chem. Phys.*, 1975, **62**, 2502–2504.
36 A. B. Elkowitz and R. E. Wyatt, *J. Chem. Phys.*, 1975, **62**, 2504–2506.
37 E. A. McCullough and R. E. Wyatt, *J. Chem. Phys.*, 1971, **54**, 3578.
38 E. J. Heller, *J. Chem. Phys.*, 1975, **62**, 1544–1555.
39 H. D. Meyer, U. Manthe and L. S. Cederbaum, *Chem. Phys. Lett.*, 1990, **165**, 73–78.
40 W. Kohn and L. J. Sham, *Phys. Rev.*, 1965, **140**, A1133–A1138.
41 R. Car and M. Parrinello, *Phys. Rev. Lett.*, 1985, **55**, 2471–2474.
42 M. W. Schmidt, K. K. Baldridge, J. A. Boatz, S. T. Elbert, M. S. Gordon, J. H. Jensen, S. Koseki, N. Matsunaga, K. A. Nguyen, S. Su, T. L. Windus, M. Dupuis and J. A. Montgomery, *J. Comput. Chem.*, 1993, **14**, 1347–1363.
43 J. Hafner, *J. Comput. Chem.*, 2008, **29**, 2044–2078.
44 Y. Shao, Z. Gan, E. Epifanovsky, A. T. B. Gilbert, M. Wormit, J. Kussmann, A. W. Lange, A. Behn, J. Deng, X. Feng, D. Ghosh, M. Goldey, P. R. Horn, L. D. Jacobson, I. Kaliman, R. Z. Khaliullin, T. Kuś, A. Landau, J. Liu, E. I. Proynov, Y. M. Rhee, R. M. Richard, M. A. Rohrdanz, R. P. Steele, E. J. Sundstrom, H. L. Woodcock, P. M. Zimmerman, D. Zuev, B. Albrecht, E. Alguire, B. Austin, G. J. O. Beran, Y. A. Bernard, E. Berquist, K. Brandhorst, K. B. Bravaya, S. T. Brown, D. Casanova, C.-M. Chang, Y. Chen, S. H. Chien, K. D. Closser, D. L. Crittenden, M. Diedenhofen, R. A. DiStasio, H. Do, A. D. Dutoi, R. G. Edgar, S. Fatehi, L. Fusti-Molnar, A. Ghysels, A. Golubeva-Zadorozhnaya, J. Gomes, M. W. D. Hanson-Heine, P. H. P. Harbach, A. W. Hauser, E. G. Hohenstein, Z. C. Holden, T.-C. Jagau, H. Ji, B. Kaduk, K. Khistyaev, J. Kim, J. Kim, R. A. King,

P. Klunzinger, D. Kosenkov, T. Kowalczyk, C. M. Krauter, K. U. Lao, A. D. Laurent, K. V. Lawler, S. V. Levchenko, C. Y. Lin, F. Liu, E. Livshits, R. C. Lochan, A. Luenser, P. Manohar, S. F. Manzer, S.-P. Mao, N. Mardirossian, A. V. Marenich, S. A. Maurer, N. J. Mayhall, E. Neuscamman, C. M. Oana, R. Olivares-Amaya, D. P. O'Neill, J. A. Parkhill, T. M. Perrine, R. Peverati, A. Prociuk, D. R. Rehn, E. Rosta, N. J. Russ, S. M. Sharada, S. Sharma, D. W. Small, A. Sodt, T. Stein, D. Stück, Y.-C. Su, A. J. W. Thom, T. Tsuchimochi, V. Vanovschi, L. Vogt, O. Vydrov, T. Wang, M. A. Watson, J. Wenzel, A. White, C. F. Williams, J. Yang, S. Yeganeh, S. R. Yost, Z.-Q. You, I. Y. Zhang, X. Zhang, Y. Zhao, B. R. Brooks, G. K. L. Chan, D. M. Chipman, C. J. Cramer, W. A. Goddard, M. S. Gordon, W. J. Hehre, A. Klamt, H. F. Schaefer, M. W. Schmidt, C. D. Sherrill, D. G. Truhlar, A. Warshel, X. Xu, A. Aspuru-Guzik, R. Baer, A. T. Bell, N. A. Besley, J.-D. Chai, A. Dreuw, B. D. Dunietz, T. R. Furlani, S. R. Gwaltney, C.-P. Hsu, Y. Jung, J. Kong, D. S. Lambrecht, W. Liang, C. Ochsenfeld, V. A. Rassolov, L. V. Slipchenko, J. E. Subotnik, T. Van Voorhis, J. M. Herbert, A. I. Krylov, P. M. W. Gill and M. Head-Gordon, *Mol. Phys.*, 2015, **113**, 184–215.

45 F. Neese, *Wiley Interdiscip. Rev.: Comput. Mol. Sci.*, 2012, **2**, 73–78.

46 H.-J. Werner, P. J. Knowles, G. Knizia, F. R. Manby and M. Schütz, *Wiley Interdiscip. Rev.: Comput. Mol. Sci.*, 2012, **2**, 242–253.

47 I. S. Ufimtsev and T. J. Martinez, *J. Chem. Theory Comput.*, 2009, **5**, 2619–2628.

48 J. Chen, Z. G. Sun and D. H. Zhang, *J. Chem. Phys.*, 2015, **142**, 024303.

49 Z. Xie and J. M. Bowman, *J. Chem. Theory Comput.*, 2010, **6**, 26–34.

50 J. M. Bowman, G. Czako and B. N. Fu, *Phys. Chem. Chem. Phys.*, 2011, **13**, 8094–8111.

51 C. Qu, Q. Yu and J. M. Bowman, *Annu. Rev. Phys. Chem.*, 2018, **69**, 151–175.

52 C. Qu, Q. Yu, B. L. Van Hoozen, J. M. Bowman and R. A. Vargas-Hernandez, *J. Chem. Theory Comput.*, 2018, **14**, 3381–3396.

53 A. Nandi, C. Qu, P. L. Houston, R. Conte and J. M. Bowman, *J. Chem. Phys.*, 2021, **154**, 051102.

54 O. T. Unke and M. Meuwly, *J. Chem. Inf. Model.*, 2017, **57**, 1923–1931.

55 D. Koner, J. C. S. Veliz, R. J. Bemish and M. Meuwly, *Phys. Chem. Chem. Phys.*, 2020, **22**, 18488–18498.

56 M. Meuwly, *Chem. Rev.*, 2021, **121**, 10218–10239.

57 K. M. Thompson, Y. D. Gao, P. Marshall, H. Wang, L. S. Zhou, Y. L. Li and H. Guo, *J. Chem. Phys.*, 2017, **147**, 134302.

58 S. Mallikarjun Sharada, T. Bligaard, A. C. Luntz, G.-J. Kroes and J. K. Nørskov, *J. Phys. Chem. C*, 2017, **121**, 19807–19815.

59 T. Tchakoua, T. Jansen, Y. van Nies, R. F. A. van den Elshout, B. A. B. van Boxmeer, S. P. Poort, M. G. Ackermans, G. S. Beltrao, S. A. Hildebrand, S. E. J. Beekman, T. van der Drift, S. Kaart, A. Santic, E. E. Spuijbroek, N. Gerrits, M. F. Somers and G.-J. Kroes, *J. Phys. Chem. A*, 2023, **127**, 10481–10498.

60 B. Jiang, J. Li and H. Guo, *J. Phys. Chem. Lett.*, 2020, **11**, 5120–5131.

61 W. G. Stark, J. Westermayr, O. A. Douglas-Gallardo, J. Gardner, S. Habershon and R. J. Maurer, *J. Phys. Chem. C*, 2023, **127**, 24168–24182.

62 J. Behler, *Angew. Chem., Int. Ed.*, 2017, **56**, 12828–12840.

63 J. Behler, *J. Chem. Phys.*, 2016, **145**, 170901.

64 J. Behler and M. Parrinello, *Phys. Rev. Lett.*, 2007, **98**, 146401.
65 T. J. Frankcombe, M. A. Collins and D. H. Zhang, *J. Chem. Phys.*, 2012, **137**, 144701.
66 R. P. A. Bettens and M. A. Collins, *J. Chem. Phys.*, 1999, **111**, 816–826.
67 N. Hertl, A. Kandratsenka and A. M. Wodtke, *Phys. Chem. Chem. Phys.*, 2022, **24**, 8738–8748.
68 S. M. Janke, D. J. Auerbach, A. M. Wodtke and A. Kandratsenka, *J. Chem. Phys.*, 2015, **143**, 124708.
69 M. Kammler, S. M. Janke, A. Kandratsenka and A. M. Wodtke, *Chem. Phys. Lett.*, 2017, **683**, 286–290.
70 D. H. Zhang and H. Guo, *Annu. Rev. Phys. Chem.*, 2016, **67**, 135–158.
71 B. Fu and D. H. Zhang, *J. Chem. Theory Comput.*, 2018, **14**, 2289–2303.
72 Z. G. Sun and D. H. Zhang, *Prog. Chem.*, 2012, **24**, 1153–1165.
73 Z. G. Sun, W. T. Yang and D. H. Zhang, *Phys. Chem. Chem. Phys.*, 2012, **14**, 1827–1845.
74 G. G. Balint-Kurti, *Theor. Chem. Acc.*, 2010, **127**, 1–17.
75 Z. G. Sun, H. Guo and D. H. Zhang, *J. Chem. Phys.*, 2010, **132**, 084112.
76 H. L. Zhao, X. X. Hu, D. Q. Xie and Z. G. Sun, *J. Chem. Phys.*, 2018, **149**, 174103.
77 D. C. Clary, *Faraday Discuss.*, 2018, **212**, 9–32.
78 H. D. Meyer, *Wiley Interdiscip. Rev.: Comput. Mol. Sci.*, 2012, **2**, 351–374.
79 U. Manthe, *J. Phys.: Condens.Matter*, 2017, **29**, 253001.
80 B. Zhao, Z. G. Sun and H. Guo, *J. Chem. Phys.*, 2014, **140**, 234110.
81 L. Dupuy, D. Lauvergnat and Y. Scribano, *Chem. Phys. Lett.*, 2022, **787**, 139241.
82 G. J. Kroes, *Phys. Chem. Chem. Phys.*, 2012, **14**, 14966–14981.
83 G. J. Kroes, *Phys. Chem. Chem. Phys.*, 2021, **23**, 8962–9048.
84 G.-J. Kroes and C. Díaz, *Chem. Soc. Rev.*, 2016, **45**, 3658–3700.
85 J. W. Lu, B. S. Day, L. R. Fiegland, E. D. Davis, W. A. Alexander, D. Troya and J. R. Morris, *Prog. Surf. Sci.*, 2012, **87**, 221–252.
86 M. A. Tesa-Serrate, E. J. Smoll, T. K. Minton and K. G. McKendrick, *Annu. Rev. Phys. Chem.*, 2016, **67**, 515–540.
87 L. Shi, M. Schröder, H.-D. Meyer, D. Peláez, A. M. Wodtke, K. Golibrzuch, A.-M. Schönemann, A. Kandratsenka and F. Gatti, *J. Chem. Phys.*, 2023, **159**, 194102.
88 L. Zhang, J. Zuo, Y. V. V. Suleimanov and H. Guo, *J. Phys. Chem. Lett.*, 2023, **14**, 7118–7125.
89 C. Li, Y. Li and B. Jiang, *Chem. Sci.*, 2023, **14**, 5087–5098.
90 B. K. Kendrick, *J. Chem. Phys.*, 2018, **148**, 069902.
91 D. Koner, R. J. Bemish and M. Meuwly, *J. Phys. Chem. A*, 2020, **124**, 6255–6269.
92 M. Blanco-Rey, J. I. Juaristi, R. Díez Muiño, H. F. Busnengo, G. J. Kroes and M. Alducin, *Phys. Rev. Lett.*, 2014, **112**, 103203.
93 P. Spiering, K. Shakouri, J. Behler, G.-J. Kroes and J. Meyer, *J. Phys. Chem. Lett.*, 2019, **10**, 2957–2962.
94 Y. L. Zhang, R. J. Maurer, H. Guo and B. Jiang, *Chem. Sci.*, 2019, **10**, 1089–1097.
95 J. I. Juaristi, M. Alducin, R. D. Muiño, H. F. Busnengo and A. Salin, *Phys. Rev. Lett.*, 2008, **100**, 116102.
96 M. Pavanello, D. J. Auerbach, A. M. Wodtke, M. Blanco-Rey, M. Alducin and G. J. Kroes, *J. Phys. Chem. Lett.*, 2013, **4**, 3735–3740.

97 M. Askerka, R. J. Maurer, V. S. Batista and J. C. Tully, *Phys. Rev. Lett.*, 2016, **116**, 217601.
98 R. J. Maurer, M. Askerka, V. S. Batista and J. C. Tully, *Phys. Rev. B*, 2016, **94**, 115432.
99 Y. L. Zhang, R. J. Maurer and B. Jiang, *J. Phys. Chem. C*, 2020, **124**, 186–195.
100 C. L. Box, Y. Zhang, R. Yin, B. Jiang and R. J. Maurer, *JACS Au*, 2021, **1**, 164–173.
101 Y. Zhang, C. L. Box, T. Schaefer, A. Kandratsenka, A. M. Wodtke, R. J. Maurer and B. Jiang, *Phys. Chem. Chem. Phys.*, 2022, **24**, 19753–19760.
102 E. Rutherford, *Philos. Mag.*, 1911, **21**, 669–688.
103 J. J. Lin, D. W. Hwang, S. Harich, Y. T. Lee and X. M. Yang, *Rev. Sci. Instrum.*, 1998, **69**, 1642–1646.
104 X. Yang, J. Lin, Y. T. Lee, D. A. Blank, A. G. Suits and A. M. Wodtke, *Rev. Sci. Instrum.*, 1997, **68**, 3317–3326.
105 P. A. Willis, H. U. Stauffer, R. Z. Hinrichs and H. F. Davis, *Rev. Sci. Instrum.*, 1999, **70**, 2606–2614.
106 D. R. Albert and H. F. Davis, *Phys. Chem. Chem. Phys.*, 2013, **15**, 14566–14580.
107 D. R. Albert, M. A. Todt and H. F. Davis, *J. Phys. Chem. A*, 2013, **117**, 13967–13975.
108 N. Balucani, G. Capozza, F. Leonori, E. Segoloni and P. Casavecchia, *Int. Rev. Phys. Chem.*, 2006, **25**, 109–163.
109 J. L. Hall, E. J. Robinson and L. M. Branscomb, *Phys. Rev. Lett.*, 1965, **14**, 1013.
110 R. A. Fox, R. M. Kogan and E. J. Robinson, *Phys. Rev. Lett.*, 1971, **26**, 1416.
111 B. Held, C. Manus, G. Mainfray and J. Morellec, *Phys. Rev. Lett.*, 1972, **28**, 130.
112 B. Held, G. Mainfray, C. Manus, J. Morellec and F. Sanchez, *Phys. Rev. Lett.*, 1973, **30**, 423–426.
113 W. C. Lineberger and T. A. Patterson, *Chem. Phys. Lett.*, 1972, **13**, 40.
114 C. B. Collins, B. W. Johnson, D. Popescu, G. Musa, M. L. Pascu and I. Popescu, *Phys. Rev. A*, 1973, **8**, 2197–2201.
115 P. M. Johnson, M. R. Berman and D. Zakheim, *J. Chem. Phys.*, 1975, **62**, 2500–2502.
116 G. Petty, C. Tai and F. W. Dalby, *Phys. Rev. Lett.*, 1975, **34**, 1207–1209.
117 P. M. Johnson, *J. Chem. Phys.*, 1976, **64**, 4143–4148.
118 D. H. Parker, S. J. Sheng and M. A. El-Sayed, *J. Chem. Phys.*, 1976, **65**, 5534–5535.
119 A. J. R. Heck and D. W. Chandler, *Annu. Rev. Phys. Chem.*, 1995, **46**, 335–372.
120 D. W. Chandler and P. L. Houston, *J. Chem. Phys.*, 1987, **87**, 1445–1447.
121 M. A. Buntine, D. P. Baldwin, R. N. Zare and D. W. Chandler, *J. Chem. Phys.*, 1991, **94**, 4672–4675.
122 T. N. Kitsopoulos, M. A. Buntine, D. P. Baldwin, R. N. Zare and D. W. Chandler, *Science*, 1993, **260**, 1605–1610.
123 A. Eppink and D. H. Parker, *Rev. Sci. Instrum.*, 1997, **68**, 3477–3484.
124 C. R. Gebhardt, T. P. Rakitzis, P. C. Samartzis, V. Ladopoulos and T. N. Kitsopoulos, *Rev. Sci. Instrum.*, 2001, **72**, 3848–3853.
125 D. Townsend, M. P. Minitti and A. G. Suits, *Rev. Sci. Instrum.*, 2003, **74**, 2530–2539.
126 J. J. Lin, J. G. Zhou, W. C. Shiu and K. P. Liu, *Rev. Sci. Instrum.*, 2003, **74**, 2495–2500.

127 M. N. R. Ashfold, N. H. Nahler, A. J. Orr-Ewing, O. P. J. Vieuxmaire, R. L. Toomes, T. N. Kitsopoulos, I. A. Garcia, D. A. Chestakov, S. M. Wu and D. H. Parker, *Phys. Chem. Chem. Phys.*, 2006, **8**, 26–53.
128 D. Yuan, W. Chen, C. Luo, Y. Tan, S. Li, Y. Huang, Z. Sun, X. Yang and X. Wang, *J. Phys. Chem. Lett.*, 2020, **11**, 1222–1227.
129 C. S. Slater, S. Blake, M. Brouard, A. Lauer, C. Vallance, J. J. John, R. Turchetta, A. Nomerotski, L. Christensen, J. H. Nielsen, M. P. Johansson and H. Stapelfeldt, *Phys. Rev. A*, 2014, **89**, 011401.
130 A. Nomerotski, M. Brouard, E. Campbell, A. Clark, J. Crooks, J. Fopma, J. J. John, A. J. Johnsen, C. Slater, R. Turchetta, C. Vallance, E. Wilman and W. H. Yuen, *J. Instrum.*, 2010, **5**, C07007.
131 L. Schnieder, W. Meier, K. H. Welge, M. N. R. Ashfold and C. M. Western, *J. Chem. Phys.*, 1990, **92**, 7027–7037.
132 L. Schnieder, K. Seekamprahn, J. Borkowski, E. Wrede, K. H. Welge, F. J. Aoiz, L. Banares, M. J. Dmello, V. J. Herrero, V. S. Rabanos and R. E. Wyatt, *Science*, 1995, **269**, 207–210.
133 L. Schnieder, K. SeekampRahn, E. Wrede and K. H. Welge, *J. Chem. Phys.*, 1997, **107**, 6175–6195.
134 B. R. Strazisar, C. Lin and H. F. Davis, *Science*, 2000, **290**, 958–961.
135 S. D. Chao, S. A. Harich, D. X. Dai, C. C. Wang, X. M. Yang and R. T. Skodje, *J. Chem. Phys.*, 2002, **117**, 8341–8361.
136 S. A. Harich, D. Dai, X. M. Yang, S. D. Chao and R. T. Skodje, *J. Chem. Phys.*, 2002, **116**, 4769–4772.
137 D. X. Dai, C. C. Wang, S. A. Harich, X. Y. Wang, X. M. Yang, S. D. Chao and R. T. Skodje, *Science*, 2003, **300**, 1730–1734.
138 M. H. Qiu, L. Che, Z. F. Ren, D. X. Dai, X. Y. Wang and X. M. Yang, *Rev. Sci. Instrum.*, 2005, **76**, 083107.
139 J. Y. Zhang, D. X. Dai, C. C. Wang, S. A. Harich, X. Y. Wang, X. M. Yang, M. Gustafsson and R. T. Skodje, *Phys. Rev. Lett.*, 2006, **96**, 093201.
140 R. N. Dixon, D. W. Hwang, X. F. Yang, S. Harich, J. J. Lin and X. Yang, *Science*, 1999, **285**, 1249–1253.
141 M. N. R. Ashfold, B. Cronin, A. L. Devine, R. N. Dixon and M. G. D. Nix, *Science*, 2006, **312**, 1637–1640.
142 G. Sun, X. F. Zheng, K. S. Xu, Y. Song and J. S. Zhang, *J. Phys. Chem. A*, 2021, **125**, 8882–8890.
143 Y. Nagaya, H. Nakatsu, S. Ogura, K. Shimazaki, H. Ueta, K. Takeyasu and K. Fukutani, *J. Chem. Phys.*, 2021, **155**, 194201.
144 R. I. Kaiser, C. Ochsenfeld, M. Head-Gordon, Y. T. Lee and A. G. Suits, *Science*, 1996, **274**, 1508–1511.
145 R. I. Kaiser and A. M. Mebel, *Int. Rev. Phys. Chem.*, 2002, **21**, 307–356.
146 R. I. Kaiser, D. S. N. Parker and A. M. Mebel, *Annu. Rev. Phys. Chem.*, 2015, **66**, 43–67.
147 Z. Zhao, Y. Wang, X. Yang, J. Quan, B. C. Krueger, P. Stoicescu, R. Nieman, D. J. Auerbach, A. M. Wodtke, H. Guo and G. B. Park, *Nat. Chem.*, 2023, **15**, 1006–1011.
148 Z. F. Ren, M. H. Qiu, L. Che, D. X. Dai, X. Y. Wang and X. M. Yang, *Rev. Sci. Instrum.*, 2006, **77**, 016102.
149 J. J. Valentini, M. J. Coggiola and Y. T. Lee, *Rev. Sci. Instrum.*, 1977, **48**, 58–63.

150 H. F. Davis, J. Shu, D. S. Peterka and M. Ahmed, *J. Chem. Phys.*, 2004, **121**, 6254–6257.
151 R. I. Kaiser, N. Balucani, D. O. Charkin and A. M. Mebel, *Chem. Phys. Lett.*, 2003, **382**, 112–119.
152 S.-H. Lee, W.-J. Huang, Y.-C. Lin and C.-H. Chin, *Astrophys. J.*, 2012, **759**, 75–84.
153 W.-J. Huang, Y.-L. Sun, C.-H. Chin and S.-H. Lee, *J. Chem. Phys.*, 2014, **141**, 124314.
154 F. Stahl, P. von Ragué Schleyer, H. F. Bettinger, R. I. Kaiser, Y. T. Lee and H. F. Schaefer III, *J. Chem. Phys.*, 2001, **114**, 3476–3487.
155 R. G. Macdonald, K. P. Liu, D. M. Sonnenfroh and D. J. Liu, *Can. J. Chem.*, 1994, **72**, 660–672.
156 R. G. Macdonald and K. P. Liu, *J. Phys. Chem.*, 1991, **95**, 9630–9633.
157 S. Y. T. van de Meerakker, N. Vanhaecke, M. P. J. van der Loo, G. C. Groenenboom and G. Meijer, *Phys. Rev. Lett.*, 2005, **95**, 013003.
158 T. K. Minton, K. P. Giapis and T. Moore, *J. Phys. Chem. A*, 1997, **101**, 6549–6555.
159 J. M. Zhang, D. J. Garton and T. K. Minton, *J. Chem. Phys.*, 2002, **117**, 6239–6251.
160 N. Bartels, T. Schäfer, J. Huhnert, R. W. Field and A. M. Wodtke, *J. Chem. Phys.*, 2012, **136**, 214201.
161 N. Bartels, B. C. Krüger, S. Meyer, A. M. Wodtke and T. Schäfer, *J. Phys. Chem. Lett.*, 2013, **4**, 2367–2370.
162 P. R. Shirhatti, I. Rahinov, K. Golibrzuch, J. Werdecker, J. Geweke, J. Altschaffel, S. Kumar, D. J. Auerbach, C. Bartels and A. M. Wodtke, *Nat. Chem.*, 2018, **10**, 592–598.
163 J. Geweke, P. R. Shirhatti, I. Rahinov, C. Bartels and A. M. Wodtke, *J. Chem. Phys.*, 2016, **145**, 054709.
164 I. Rahinov, R. Cooper, C. Yuan, X. M. Yang, D. J. Auerbach and A. M. Wodtke, *J. Chem. Phys.*, 2008, **129**, 214708.
165 T. Schäfer, N. Bartels, N. Hocke, X. M. Yang and A. M. Wodtke, *Chem. Phys. Lett.*, 2012, **535**, 1–11.
166 B. L. Yoder, R. Bisson, P. M. Hundt and R. D. Beck, *J. Chem. Phys.*, 2011, **135**, 224703.
167 K. Liu, *Annu. Rev. Phys. Chem.*, 2016, **67**, 91–111.
168 W. E. Perreault, N. Mukherjee and R. N. Zare, *J. Chem. Phys.*, 2019, **150**, 174301.
169 Y. Wang, J. Huang, W. Wang, T. Du, Y. Xie, Y. Ma, C. Xiao, Z. Zhaojun, D. H. Zhang and X. Yang, *Science*, 2023, **379**, 191–195.
170 E. Wrede, L. Schnieder, K. H. Welge, F. J. Aoiz, L. Banares, J. F. Castillo, B. Martinez-Haya and V. J. Herrero, *J. Chem. Phys.*, 1999, **110**, 9971–9981.
171 J. Jankunas, M. Sneha, R. N. Zare, F. Bouakline and S. C. Althorpe, *J. Chem. Phys.*, 2013, **139**, 144316.
172 H. Gao, M. Sneha, F. Bouakline, S. C. Althorpe and R. N. Zare, *J. Phys. Chem. A*, 2015, **119**, 12036–12042.
173 R. E. Continetti, B. A. Balko and Y. T. Lee, *J. Chem. Phys.*, 1990, **93**, 5719–5740.
174 S. A. Harich, D. X. Dai, C. C. Wang, X. M. Yang, S. D. Chao and R. T. Skodje, *Nature*, 2002, **419**, 281–284.

175 D. Yuan, Y. Guan, W. Chen, H. Zhao, S. Yu, C. Luo, Y. Tan, T. Xie, X. Wang, Z. Sun, D. H. Zhang and X. Yang, *Science*, 2018, **362**, 1289.
176 D. F. Yuan, S. R. Yu, W. T. Chen, J. W. Sang, C. Luo, T. Wang, X. Xu, P. Casavecchia, X. A. Wang, Z. G. Sun, D. H. Zhang and X. M. Yang, *Nat. Chem.*, 2018, **10**, 653–658.
177 G. C. Schatz and A. Kuppermann, *J. Chem. Phys.*, 1973, **59**, 964–965.
178 J. Z. H. Zhang, S. I. Chu and W. H. Miller, *J. Chem. Phys.*, 1988, **88**, 6233–6239.
179 R. T. Skodje and X. M. Yang, *Int. Rev. Phys. Chem.*, 2004, **23**, 253–287.
180 D. C. Chatfield, S. L. Mielke, T. C. Allison and D. G. Truhlar, *J. Chem. Phys.*, 2000, **112**, 8387–8408.
181 C. A. Mead and D. G. Truhlar, *J. Chem. Phys.*, 1979, **70**, 2284–2296.
182 D. F. Yuan, Y. Huang, W. T. Chen, H. L. Zhao, S. R. Yu, C. Luo, Y. X. Tan, S. W. Wang, X. G. Wang, Z. G. Sun and X. M. Yang, *Nat. Commun.*, 2020, **11**, 7.
183 B. Lepetit, Z. Peng and A. Kuppermann, *Chem. Phys. Lett.*, 1990, **166**, 572–580.
184 Y. S. M. Wu, A. Kuppermann and B. Lepetit, *Chem. Phys. Lett.*, 1991, **186**, 319–328.
185 E. Wrede and L. Schnieder, *J. Chem. Phys.*, 1997, **107**, 786–790.
186 M. P. de Miranda, D. C. Clary, J. F. Castillo and D. E. Manolopoulos, *J. Chem. Phys.*, 1998, **108**, 3142–3153.
187 B. K. Kendrick, *J. Chem. Phys.*, 2000, **112**, 5679–5704.
188 J. C. Juanes-Marcos and S. C. Althorpe, *J. Chem. Phys.*, 2005, **122**, 204324.
189 B. K. Kendrick, *J. Phys. Chem. A*, 2003, **107**, 6739–6756.
190 J. C. Juanes-Marcos, S. C. Althorpe and E. Wrede, *Science*, 2005, **309**, 1227–1230.
191 S. C. Althorpe, *J. Chem. Phys.*, 2006, **124**, 084105.
192 F. Bouakline, S. C. Althorpe and D. P. Ruiz, *J. Chem. Phys.*, 2008, **128**, 124322.
193 B. K. Kendrick, J. Hazra and N. Balakrishnan, *Phys. Rev. Lett.*, 2015, **115**, 153201.
194 S. F. Wu, B. R. Johnson and R. D. Levine, *Mol. Phys.*, 1973, **25**, 839–856.
195 G. C. Schatz, J. M. Bowman and A. Kuppermann, *J. Chem. Phys.*, 1973, **58**, 4023–4025.
196 D. M. Neumark, A. M. Wodtke, G. N. Robinson, C. C. Hayden and Y. T. Lee, *Phys. Rev. Lett.*, 1984, **53**, 226–229.
197 F. J. Aoiz, L. Banares, V. J. Herrero, V. S. Rabanos, K. Stark and H. J. Werner, *Chem. Phys. Lett.*, 1994, **223**, 215–226.
198 J. F. Castillo, D. E. Manolopoulos, K. Stark and H. J. Werner, *J. Chem. Phys.*, 1996, **104**, 6531–6546.
199 R. T. Skodje, D. Skouteris, D. E. Manolopoulos, S. H. Lee, F. Dong and K. P. Liu, *Phys. Rev. Lett.*, 2000, **85**, 1206–1209.
200 T. G. Yang, L. Huang, C. L. Xiao, J. Chen, T. Wang, D. X. Dai, F. Lique, M. H. Alexander, Z. G. Sun, D. H. Zhang, X. M. Yang and D. M. Neumark, *Nat. Chem.*, 2019, **11**, 744–749.
201 D. E. Manolopoulos, K. Stark, H. J. Werner, D. W. Arnold, S. E. Bradforth and D. M. Neumark, *Science*, 1993, **262**, 1852–1855.
202 M. H. Qiu, Z. F. Ren, L. Che, D. X. Dai, S. A. Harich, X. Y. Wang, X. M. Yang, C. X. Xu, D. Q. Xie, M. Gustafsson, R. T. Skodje, Z. G. Sun and D. H. Zhang, *Science*, 2006, **311**, 1440–1443.

203 Z. F. Ren, L. Che, M. H. Qiu, X. A. Wang, W. R. Dong, D. X. Dai, X. Y. Wang, X. M. Yang, Z. G. Sun, B. Fu, S. Y. Lee, X. Xu and D. H. Zhang, *Proc. Natl. Acad. Sci. U.S.A.*, 2008, **105**, 12662–12666.
204 J. B. Kim, M. L. Weichman, T. F. Sjolander, D. M. Neumark, J. Klos, M. H. Alexander and D. E. Manolopoulos, *Science*, 2015, **349**, 510–513.
205 T. Wang, T. G. Yang, C. L. Xiao, Z. G. Sun, D. H. Zhang, X. M. Yang, M. L. Weichman and D. M. Neumark, *Chem. Soc. Rev.*, 2018, **47**, 6744–6763.
206 W. R. Dong, C. L. Xiao, T. Wang, D. X. Dai, X. M. Yang and D. H. Zhang, *Science*, 2010, **327**, 1501–1502.
207 M. Alagia, N. Balucani, L. Cartechini, P. Casavecchia, G. G. Volpi, F. J. Aoiz, L. Bañares, T. C. Allison, S. L. Mielke and D. G. Truhlar, *Phys. Chem. Chem. Phys.*, 2000, **2**, 599–612.
208 M. Alagia, N. Balucani, L. Cartechini, P. Casavecchia, E. H. vanKleef, G. G. Volpi, F. J. Aoiz, L. Banares, D. W. Schwenke, T. C. Allison, S. L. Mielke and D. G. Truhlar, *Science*, 1996, **273**, 1519–1522.
209 X. G. Wang, W. R. Dong, C. L. Xiao, L. Che, Z. F. Ren, D. X. Dai, X. Y. Wang, P. Casavecchia, X. M. Yang, B. Jiang, D. Q. Xie, Z. G. Sun, S. Y. Lee, D. H. Zhang, H. J. Werner and M. H. Alexander, *Science*, 2008, **322**, 573–576.
210 N. Balucani, G. Capozza, E. Segoloni, A. Russo, R. Bobbenkamp, P. Casavecchia, T. Gonzalez-Lezana, E. J. Rackham, L. Bañares and F. J. Aoiz, *J. Chem. Phys.*, 2005, **122**, 234309.
211 S. A. Lahankar, J. M. Zhang, K. G. McKendrick and T. K. Minton, *Nat. Chem.*, 2013, **5**, 315–319.
212 M. Alagia, N. Balucani, L. Cartechini, P. Casavecchia, E. H. van Kleef, G. G. Volpi, P. J. Kuntz and J. J. Sloan, *J. Chem. Phys.*, 1998, **108**, 6698–6708.
213 X. H. Liu, J. J. Lin, S. Harich, G. C. Schatz and X. M. Yang, *Science*, 2000, **289**, 1536–1538.
214 M. Alagia, N. Balucani, L. Cartechini, P. Casavecchia, G. G. Volpi, L. A. Pederson, G. C. Schatz, G. Lendvay, L. B. Harding, T. Hollebeek, T. S. Ho and H. Rabitz, *J. Chem. Phys.*, 1999, **110**, 8857–8860.
215 C. L. Xiao, X. Xu, S. Liu, T. Wang, W. R. Dong, T. G. Yang, Z. G. Sun, D. X. Dai, X. Xu, D. H. Zhang and X. M. Yang, *Science*, 2011, **333**, 440–442.
216 P. Casavecchia, F. Leonori and N. Balucani, *Int. Rev. Phys. Chem.*, 2015, **34**, 161–204.
217 J. J. Lin, J. G. Zhou, W. C. Shiu and K. P. Liu, *Science*, 2003, **300**, 966–969.
218 J. G. Zhou, J. J. Lin, W. C. Shiu and K. P. Liu, *J. Chem. Phys.*, 2003, **119**, 4997–5000.
219 W. Shiu, J. J. Lin and K. P. Liu, *Phys. Rev. Lett.*, 2004, **92**, 103201.
220 J. G. Zhou, J. J. Lin and K. P. Liu, *J. Chem. Phys.*, 2003, **119**, 8289–8296.
221 J. Y. Yang, D. Zhang, B. Jiang, D. X. Dai, G. R. Wu, D. H. Zhang and X. M. Yang, *J. Phys. Chem. Lett.*, 2014, **5**, 1790–1794.
222 W. Shiu, J. J. Lin, K. P. Liu, M. Wu and D. H. Parker, *J. Chem. Phys.*, 2004, **120**, 117–122.
223 Z. Chen, J. Chen, R. J. Chen, T. Xie, X. G. Wang, S. Liu, G. R. Wu, D. X. Dai, X. M. Yang and D. H. Zhang, *Proc. Natl. Acad. Sci. U.S.A.*, 2020, **117**, 9202–9207.
224 G. R. Wu, W. Q. Zhang, H. L. Pan, Q. A. Shuai, J. Y. Yang, B. Jiang, D. X. Dai and X. M. Yang, *Phys. Chem. Chem. Phys.*, 2010, **12**, 9469–9474.

225 W. Q. Zhang, G. R. Wu, H. L. Pan, Q. Shuai, B. Jiang, D. X. Dai and X. M. Yang, *J. Phys. Chem. A*, 2009, **113**, 4652–4657.
226 W. Q. Zhang, Y. Zhou, G. R. Wu, Y. P. Lu, H. L. Pan, B. N. Fu, Q. A. Shuai, L. Liu, S. Liu, L. L. Zhang, B. Jiang, D. X. Dai, S. Y. Lee, Z. Xie, B. J. Braams, J. M. Bowman, M. A. Collins, D. H. Zhang and X. M. Yang, *Proc. Natl. Acad. Sci. U.S.A.*, 2010, **107**, 12782–12785.
227 J. Y. Yang, K. J. Shao, D. Zhang, Q. Shuai, B. N. Fu, D. H. Zhang and X. M. Yang, *J. Phys. Chem. Lett.*, 2014, **5**, 3106–3111.
228 J. J. Lin, J. Shu, Y. T. Lee and X. Yang, *J. Chem. Phys.*, 2000, **113**, 5287–5301.
229 P. Casavecchia, G. Capozza, E. Segoloni, F. Leonori, N. Balucani and G. G. Volpi, *J. Phys. Chem. A*, 2005, **109**, 3527–3530.
230 B. N. Fu, Y. C. Han, J. M. Bowman, L. Angelucci, N. Balucani, F. Leonori and P. Casavecchia, *Proc. Natl. Acad. Sci. U.S.A.*, 2012, **109**, 9733–9738.
231 F. Leonori, A. Occhiogrosso, N. Balucani, A. Bucci, R. Petrucci and P. Casavecchia, *J. Phys. Chem. Lett.*, 2012, **3**, 75–80.
232 P. Recio, S. Alessandrini, G. Vanuzzo, G. Pannacci, A. Baggioli, D. Marchione, A. Caracciolo, V. J. Murray, P. Casavecchia, N. Balucani, C. Cavallotti, C. Puzzarini and V. Barone, *Nat. Chem.*, 2022, **14**, 1405–1412.
233 C. Cavallotti, A. Della Libera, C. W. Zhou, P. Recio, A. Caracciolo, N. Balucani and P. Casavecchia, *Faraday Discuss.*, 2022, **238**, 161–182.
234 B. B. Dangi, D. S. N. Parker, R. I. Kaiser, D. Belisario-Lara and A. M. Mebel, *Chem. Phys. Lett.*, 2014, **607**, 92–99.
235 D. S. N. Parker, S. Maity, B. B. Dangi, R. I. Kaiser, A. Landera and A. M. Mebel, *Phys. Chem. Chem. Phys.*, 2014, **16**, 12150–12163.
236 D. S. N. Parker, T. Yang, R. I. Kaiser, A. Landera and A. M. Mebel, *Chem. Phys. Lett.*, 2014, **595–596**, 230–236.
237 T. Yang, B. B. Dangi, D. S. N. Parker, R. I. Kaiser, Y. An and A. H. H. Chang, *Phys. Chem. Chem. Phys.*, 2014, **16**, 17580–17587.
238 T. Yang, B. B. Dangi, P. Maksyutenko, R. I. Kaiser, L. W. Bertels and M. Head-Gordon, *J. Phys. Chem. A*, 2015, **119**, 12562–12578.
239 T. Yang, B. B. Dangi, R. I. Kaiser, L. W. Bertels and M. Head-Gordon, *J. Phys. Chem. A*, 2016, **120**, 4872–4883.
240 M. Lucas, A. M. Thomas, R. I. Kaiser, E. K. Bashkirov, V. N. Azyazov and A. M. Mebel, *J. Phys. Chem. A*, 2018, **122**, 3128–3139.
241 A. M. Thomas, M. Lucas, L. Zhao, J. Liddiard, R. I. Kaiser and A. M. Mebel, *Phys. Chem. Chem. Phys.*, 2018, **20**, 10906–10925.
242 C. He, L. Zhao, A. M. Thomas, G. R. Galimova, A. M. Mebel and R. I. Kaiser, *Phys. Chem. Chem. Phys.*, 2019, **21**, 22308–22319.
243 C. He, L. Zhao, A. M. Thomas, A. N. Morozov, A. M. Mebel and R. I. Kaiser, *J. Phys. Chem. A*, 2019, **123**, 5446–5462.
244 C. He, G. R. Galimova, Y. Luo, L. Zhao, A. K. Eckhardt, R. Sun, A. M. Mebel and R. I. Kaiser, *Proc. Natl. Acad. Sci. U.S.A.*, 2020, **117**, 30142–30150.
245 C. He, S. J. Goettl, Z. Yang, S. Doddipatla, R. I. Kaiser, M. X. Silva and B. R. L. Galvao, *Phys. Chem. Chem. Phys.*, 2021, **23**, 18506–18516.
246 Z. Yang, C. He, S. Goettl and R. I. Kaiser, *J. Phys. Chem. A*, 2021, **125**, 5040–5047.
247 G. R. Galimova, A. M. Mebel, S. J. Goettl, Z. Yang and R. I. Kaiser, *Phys. Chem. Chem. Phys.*, 2022, **24**, 22453–22463.

248 S. J. Goettl, C. He, D. Paul, A. A. Nikolayev, V. N. Azyazov, A. M. Mebel and R. I. Kaiser, *J. Phys. Chem. A*, 2022, **126**, 1889–1898.
249 C. He, S. J. Goettl, Z. Yang, R. I. Kaiser, A. A. Nikolayev, V. N. Azyazov and A. M. Mebel, *J. Phys. Chem. Lett.*, 2022, **13**, 4589–4597.
250 C. He, Z. Yang, S. Doddipatla, A. M. Thomas, R. I. Kaiser, G. R. Galimova, A. M. Mebel, K. Fujioka and R. Sun, *Phys. Chem. Chem. Phys.*, 2022, **24**, 26499–26510.
251 L. B. Tuli, S. J. Goettl, A. M. Turner, A. H. Howlader, P. Hemberger, S. F. Wnuk, T. Guo, A. M. Mebel and R. I. Kaiser, *Nat. Commun.*, 2023, **14**, 1527.
252 G. Vanuzzo, A. Caracciolo, T. K. Minton, N. Balucani, P. Casavecchia, C. de Falco, A. Baggioli and C. Cavallotti, *J. Phys. Chem. A*, 2021, **125**, 8434–8453.
253 A. V. Wilson, D. S. N. Parker, F. T. Zhang and R. I. Kaiser, *Phys. Chem. Chem. Phys.*, 2012, **14**, 477–481.
254 F. T. Zhang, P. Maksyutenko and R. I. Kaiser, *Phys. Chem. Chem. Phys.*, 2012, **14**, 529–537.
255 N. Balucani, *Chem. Soc. Rev.*, 2012, **41**, 5473–5483.
256 T. Yang, L. Bertels, B. B. Dangi, X. Li, M. Head-Gordon and R. I. Kaiser, *Proc. Natl. Acad. Sci. U.S.A.*, 2019, **116**, 14471–14478.
257 Z. Yang, S. Doddipatla, R. I. Kaiser, A. A. Nikolayev, V. N. Azyazov and A. M. Mebel, *Astrophys. J. Lett.*, 2021, **908**, L40.
258 L. Zhao, S. Doddipatla, R. I. Kaiser, W. Lu, O. Kostko, M. Ahmed, L. B. Tuli, A. N. Morozov, A. H. Howlader, S. F. Wnuk, A. M. Mebel, V. N. Azyazov, R. K. Mohamedf and F. R. Fischer, *Phys. Chem. Chem. Phys.*, 2021, **23**, 5740–5749.
259 N. Balucani, A. Caracciolo, G. Vanuzzo, D. Skouteris, M. Rosi, L. Pacifici, P. Casavecchia, K. M. Hickson, J. C. Loison and M. Dobrijevic, *Faraday Discuss.*, 2023, **245**, 327–351.
260 P. A. Willis, H. U. Stauffer, R. Z. Hinrichs and H. F. Davis, *J. Phys. Chem. A*, 1999, **103**, 3706–3720.
261 H. U. Stauffer, R. Z. Hinrichs, J. J. Schroden and H. F. Davis, *J. Phys. Chem. A*, 2000, **104**, 1107–1116.
262 F. F. Li, C. W. Dong, J. Chen, J. X. Liu, F. Y. Wang and X. Xu, *Chem. Sci.*, 2018, **9**, 488–494.
263 C. W. Dong, J. X. Liu, F. F. Li and F. Y. Wang, *Chin. J. Chem. Phys.*, 2016, **29**, 99–104.
264 D. Yan, Y. J. Ma, F. F. Li, J. X. Liu, G. J. Wang and F. Y. Wang, *Chin. J. Chem. Phys.*, 2020, **33**, 239–242.
265 P. A. Willis, H. U. Stauffer, R. Z. Hinrichs and H. F. Davis, *J. Chem. Phys.*, 1998, **108**, 2665–2668.
266 H. U. Stauffer, R. Z. Hinrichs, J. J. Schroden and H. F. Davis, *J. Chem. Phys.*, 1999, **111**, 10758–10761.
267 H. U. Stauffer, R. Z. Hinrichs, P. A. Willis and H. F. Davis, *J. Chem. Phys.*, 1999, **111**, 4101–4112.
268 R. Z. Hinrichs, P. A. Willis, H. U. Stauffer, J. J. Schroden and H. F. Davis, *J. Chem. Phys.*, 2000, **112**, 4634–4643.
269 J. J. Schroden, M. Teo and H. F. Davis, *J. Chem. Phys.*, 2002, **117**, 9258–9265.
270 R. Z. Hinrichs, J. J. Schroden and H. F. Davis, *J. Am. Chem. Soc.*, 2003, **125**, 860–861.

271 R. Z. Hinrichs, J. J. Schroden and H. F. Davis, *J. Phys. Chem. A*, 2003, **107**, 9284–9294.
272 J. J. Schroden, C. C. Wang and H. F. Davis, *J. Phys. Chem. A*, 2003, **107**, 9295–9300.
273 R. Z. Hinrichs, J. J. Schroden and H. F. Davis, *J. Phys. Chem. A*, 2008, **112**, 3010–3019.
274 D. L. Proctor and H. F. Davis, *Proc. Natl. Acad. Sci. U.S.A.*, 2008, **105**, 12673–12677.
275 F. F. Li, Y. J. Ma, D. Yan, A. Xu, J. X. Liu and F. Y. Wang, *J. Phys. Chem. Lett.*, 2022, **13**, 11630–11635.
276 M. Oana, Y. Nakatsuka, D. R. Albert and H. F. Davis, *J. Phys. Chem. A*, 2012, **116**, 5039–5044.
277 J. J. Schroden and H. F. Davis, *J. Phys. Chem. A*, 2012, **116**, 3508–3513.
278 J. Meyer and R. Wester, *Annu. Rev. Phys. Chem.*, 2017, **68**, 333–353.
279 J. Meyer, V. Tajti, E. Carrascosa, T. Győri, M. Stei, T. Michaelsen, B. Bastian, G. Czakó and R. Wester, *Nat. Chem.*, 2021, **13**, 977–981.
280 P. A. Robertson, D. Heathcote, D. Milesevic and C. Vallance, *J. Phys. Chem. A*, 2022, **126**, 7221–7229.
281 D. Heathcote, P. A. Robertson, A. A. Butler, C. Ridley, J. Lomas, M. M. Buffett, M. Bell and C. Vallance, *Faraday Discuss.*, 2022, **238**, 682–699.
282 H. Kockert, D. Heathcote, J. W. L. Lee and C. Vallance, *Mol. Phys.*, 2021, **119**, e1811909.
283 J. N. Bull, J. W. L. Lee and C. Vallance, *Phys. Rev. A*, 2017, **96**, 042704.
284 J. N. Bull, J. W. L. Lee and C. Vallance, *Phys. Rev. A*, 2015, **91**, 022704.
285 J. N. Bull, M. Bart, C. Vallance and P. W. Harland, *Phys. Rev. A*, 2013, **88**, 062710.
286 R. T. Jongma, G. von Helden, G. Berden and G. Meijer, *Chem. Phys. Lett.*, 1997, **270**, 304–308.
287 E. Narevicius and M. G. Raizen, *Chem. Rev.*, 2012, **112**, 4879–4889.
288 S. Y. T. van de Meerakker, H. L. Bethlem, N. Vanhaecke and G. Meijer, *Chem. Rev.*, 2012, **112**, 4828–4878.
289 P. Jansen and F. Merkt, *Prog. Nucl. Magn. Reson. Spectrosc.*, 2020, **120–121**, 118–148.
290 J. Onvlee, S. N. Vogels, A. von Zastrow, D. H. Parker and S. Y. T. van de Meerakker, *Phys. Chem. Chem. Phys.*, 2014, **16**, 15768–15779.
291 J. Onvlee, S. N. Vogels and S. Y. T. van de Meerakker, *ChemPhysChem*, 2016, **17**, 3583–3595.
292 D. Auerbach, E. E. A. Bromberg and L. Wharton, *J. Chem. Phys.*, 1966, **45**, 2160–2166.
293 H. L. Bethlem, G. Berden and G. Meijer, *Phys. Rev. Lett.*, 1999, **83**, 1558–1561.
294 H. L. Bethlem, G. Berden, A. J. A. van Roij, F. M. H. Crompvoets and G. Meijer, *Phys. Rev. Lett.*, 2000, **84**, 5744–5747.
295 F. M. H. Crompvoets, H. L. Bethlem, R. T. Jongma and G. Meijer, *Nature*, 2001, **411**, 174–176.
296 C. E. Heiner, D. Carty, G. Meijer and H. L. Bethlem, *Nat. Phys.*, 2007, **3**, 115–118.
297 S. A. Meek, H. L. Bethlem, H. Conrad and G. Meijer, *Phys. Rev. Lett.*, 2008, **100**, 153003.

298 E. Narevicius, A. Libson, M. F. Riedel, C. G. Parthey, I. Chavez, U. Even and M. G. Raizen, *Phys. Rev. Lett.*, 2007, **98**, 103201.
299 E. Narevicius, A. Libson, C. G. Parthey, I. Chavez, J. Narevicius, U. Even and M. G. Raizen, *Phys. Rev. Lett.*, 2008, **100**, 093003.
300 S. D. Hogan, D. Sprecher, M. Andrist, N. Vanhaecke and F. Merkt, *Phys. Rev. A*, 2007, **76**, 023412.
301 S. D. Hogan, A. W. Wiederkehr, H. Schmutz and F. Merkt, *Phys. Rev. Lett.*, 2008, **101**, 143001.
302 J. J. Gilijamse, S. Hoekstra, S. Y. T. van de Meerakker, G. C. Groenenboom and G. Meijer, *Science*, 2006, **313**, 1617–1620.
303 M. Kirste, L. Scharfenberg, J. Klos, F. Lique, M. H. Alexander, G. Meijer and S. Y. T. van de Meerakker, *Phys. Rev. A*, 2010, **82**, 042717.
304 L. Scharfenberg, J. Klos, P. J. Dagdigian, M. H. Alexander, G. Meijer and S. Y. T. van de Meerakker, *Phys. Chem. Chem. Phys.*, 2010, **12**, 10660–10670.
305 L. Scharfenberg, S. Y. T. van de Meerakker and G. Meijer, *Phys. Chem. Chem. Phys.*, 2011, **13**, 8448–8456.
306 S. D. S. Gordon and A. Osterwalder, *Phys. Rev. Appl.*, 2017, **7**, 044022.
307 V. Plomp, Z. Gao and S. Y. T. van de Meerakker, *Mol. Phys.*, 2021, **119**, e1814437.
308 A. B. Henson, S. Gersten, Y. Shagam, J. Narevicius and E. Narevicius, *Science*, 2012, **338**, 234–238.
309 J. Jankunas, K. Jachymski, M. Hapka and A. Osterwalder, *J. Chem. Phys.*, 2015, **142**, 164305.
310 A. Klein, Y. Shagam, W. Skomorowski, P. S. Zuchowski, M. Pawlak, L. M. C. Janssen, N. Moiseyev, S. Y. T. van de Meerakker, A. van der Avoird, C. P. Koch and E. Narevicius, *Nat. Phys.*, 2017, **13**, 35–38.
311 B. Margulis, P. Paliwal, W. Skomorowski, M. Pawlak, P. S. Zuchowski and E. Narevicius, *Phys. Rev. Res.*, 2022, **4**, 043042.
312 Q. Ma, A. van der Avoird, J. Loreau, M. H. Alexander, S. Y. T. van de Meerakker and P. J. Dagdigian, *J. Chem. Phys.*, 2015, **143**, 044312.
313 X. M. Yang and D. H. Zhang, *Acc. Chem. Res.*, 2008, **41**, 981–989.
314 P. Paliwal, A. Blech, C. P. Koch and E. Narevicius, *Nat. Commun.*, 2021, **12**, 7249.
315 T. De Jongh, M. Besemer, Q. Shuai, T. Karman, A. van der Avoird, G. C. Groenenboom and S. Y. T. van de Meerakker, *Science*, 2020, **368**, 626–630.
316 W. E. Perreault, N. Mukherjee and R. N. Zare, *Nat. Chem.*, 2018, **10**, 561–567.
317 J. F. E. Croft, N. Balakrishnan, M. Huang and H. Guo, *Phys. Rev. Lett.*, 2018, **121**, 113401.
318 S. N. Vogels, J. Onvlee, A. von Zastrow, G. C. Groenenboom, A. van der Avoird and S. Y. T. van de Meerakker, *Phys. Rev. Lett.*, 2014, **113**, 263202.
319 A. von Zastrow, J. Onvlee, S. N. Vogels, G. C. Groenenboom, A. van der Avoird and S. Y. T. van de Meerakker, *Nat. Chem.*, 2014, **6**, 216–221.
320 V. Plomp, Z. Gao, T. Cremers, M. Besemer and S. Y. T. van de Meerakker, *J. Chem. Phys.*, 2020, **152**, 091103.
321 G. Tang, M. Besemer, S. Kuijpers, G. C. Groenenboom, A. van der Avoird, T. Karman and S. Y. T. van de Meerakker, *Science*, 2023, **379**, 1031–1036.
322 Q. Shuai, T. de Jongh, M. Besemer, A. van der Avoird, G. C. Groenenboom and S. Y. T. van de Meerakker, *J. Chem. Phys.*, 2020, **153**, 244302.

323 V. Zhelyazkova, F. B. V. Martins, J. A. Agner, H. Schmutz and F. Merkt, *Phys. Rev. Lett.*, 2020, **125**, 263401.
324 S. D. Hogan, P. Allmendinger, H. Sassmannshausen, H. Schmutz and F. Merkt, *Phys. Rev. Lett.*, 2012, **108**, 063008.
325 V. Zhelyazkova, F. B. V. Martins, J. A. Agner, H. Schmutz and F. Merkt, *Phys. Chem. Chem. Phys.*, 2021, **23**, 21606–21622.
326 F. B. V. Martins, V. Zhelyazkova and F. Merkt, *New J. Phys.*, 2022, **24**, 113003.
327 V. Zhelyazkova, F. B. V. Martins and F. Merkt, *Phys. Chem. Chem. Phys.*, 2022, **24**, 16360–16373.
328 V. Zhelyazkova, F. B. V. Martins, M. Zesko and F. Merkt, *Phys. Chem. Chem. Phys.*, 2022, **24**, 2843–2858.
329 V. Zhelyazkova, F. B. V. Martins, S. Schilling and F. Merkt, *J. Phys. Chem. A*, 2023, **127**, 1458–1468.
330 D. E. Heard, *Acc. Chem. Res.*, 2018, **51**, 2620–2627.
331 R. J. Shannon, M. A. Blitz, A. Goddard and D. E. Heard, *Nat. Chem.*, 2013, **5**, 745–749.
332 A. Potapov, A. Canosa, E. Jiménez and B. Rowe, *Angew. Chem., Int. Ed.*, 2017, **56**, 8618–8640.
333 R. Wild, M. Notzold, M. Simpson, T. D. Tran and R. Wester, *Nature*, 2023, **615**, 425–429.
334 E. X. Han, W. Fang, M. Stamatakis, J. O. Richardson and J. Chen, *J. Phys. Chem. Lett.*, 2022, **13**, 3173–3181.
335 A. Choudhury, J. A. A. DeVine, S. Sinha, J. A. A. Lau, A. Kandratsenka, D. Schwarzer, P. Saalfrank and A. M. M. Wodtke, *Nature*, 2022, **612**, 691–696.
336 A. M. Wodtke, *Chem. Soc. Rev.*, 2016, **45**, 3641–3657.
337 A. M. Wodtke, J. C. Tully and D. J. Auerbach, *Int. Rev. Phys. Chem.*, 2004, **23**, 513–539.
338 G. B. Park, B. C. Krüger, D. Borodin, T. N. Kitsopoulos and A. M. Wodtke, *Rep. Prog. Phys.*, 2019, **82**, 096401.
339 H. Chadwick and R. D. Beck, *Annu. Rev. Phys. Chem.*, 2017, **68**, 39–61.
340 H. Chadwick and R. D. Beck, *Chem. Soc. Rev.*, 2016, **45**, 3576–3594.
341 A. L. Utz, *Curr. Opin. Solid State Mater. Sci.*, 2009, **13**, 4–12.
342 J. C. Tully, *Annu. Rev. Phys. Chem.*, 2000, **51**, 153–178.
343 J. C. Tully, *Acc. Chem. Res.*, 1981, **14**, 188–194.
344 G. B. Park, T. N. Kitsopoulos, D. Borodin, K. Golibrzuch, J. Neugebohren, D. J. Auerbach, C. T. Campbell and A. M. Wodtke, *Nat. Rev. Chem*, 2019, **3**, 723–732.
345 J. T. Paci, T. K. Minton and G. C. Schatz, *Acc. Chem. Res.*, 2012, **45**, 1973–1981.
346 X.-F. Gao and G. M. Nathanson, *Acc. Chem. Res.*, 2022, **55**, 3294–3302.
347 J. A. Faust and G. M. Nathanson, *Chem. Soc. Rev.*, 2016, **45**, 3609–3620.
348 O. Bünermann, A. Kandratsenka and A. M. Wodtke, *J. Phys. Chem. A*, 2021, **125**, 3059–3076.
349 O. Bünermann, H. Y. Jiang, Y. Dorenkamp, D. J. Auerbach and A. M. Wodtke, *Rev. Sci. Instrum.*, 2018, **89**, 094101.
350 H. Y. Jiang, Y. Dorenkamp, K. Krüger and O. Bünermann, *J. Chem. Phys.*, 2019, **150**, 184704.
351 Y. Dorenkamp, H. Jiang, H. Koeckert, N. Hertl, M. Kammler, S. M. Janke, A. Kandratsenka, A. M. Wodtke and O. Bünermann, *J. Chem. Phys.*, 2019, **150**, 099901.

352 Y. Dorenkamp, H. Jiang, H. Kockert, N. Hertl, M. Kammler, S. M. Janke, A. Kandratsenka, A. M. Wodtke and O. Bünermann, *J. Chem. Phys.*, 2018, **148**, 034706.
353 O. Bünermann, H. Y. Jiang, Y. Dorenkamp, A. Kandratsenka, S. M. Janke, D. J. Auerbach and A. M. Wodtke, *Science*, 2015, **350**, 1346–1349.
354 N. Hertl, K. Krüger and O. Bünermann, *Langmuir*, 2022, **38**, 14162–14171.
355 R. Martin-Barrios, N. Hertl, O. Galparsoro, A. Kandratsenka, A. M. Wodtke and P. Larregaray, *Phys. Chem. Chem. Phys.*, 2022, **24**, 20813–20819.
356 L. Lecroart, N. Hertl, Y. Dorenkamp, H. Jiang, T. N. Kitsopoulos, A. Kandratsenka, O. Bünermann and A. M. Wodtke, *J. Chem. Phys.*, 2021, **155**, 034702.
357 K. Krüger, Y. Wang, S. Tödter, F. Debbeler, A. Matveenko, N. Hertl, X. Zhou, B. Jiang, H. Guo, A. M. Wodtke and O. Bünermann, *Nat. Chem.*, 2023, **15**, 326–334.
358 K. Krüger, Y. Wang, L. Zhu, B. Jiang, H. Guo, A. M. Wodtke and O. Bünermann, *Nat. Sci.*, 2023, e20230019.
359 H. Y. Jiang, X. C. Tao, M. Kammler, F. Z. Ding, A. M. Wodtke, A. Kandratsenka, T. F. Miller and O. Bünermann, *J. Phys. Chem. Lett.*, 2021, **12**, 1991–1996.
360 H. Y. Jiang, M. Kammler, F. Z. Ding, Y. Dorenkamp, F. R. Manby, A. M. Wodtke, T. F. Miller, A. Kandratsenka and O. Bünermann, *Science*, 2019, **364**, 379.
361 N. Hertl, A. Kandratsenka, O. Bünermann and A. M. Wodtke, *J. Phys. Chem. A*, 2021, **125**, 5745–5752.
362 Y. G. Li and G. Wahnström, *Phys. Rev. Lett.*, 1992, **68**, 3444–3447.
363 Y. G. Li and G. Wahnström, *Phys. Rev. B: Condens. Matter Mater. Phys.*, 1992, **46**, 14528–14542.
364 A. Kandratsenka, H. Y. Jiang, Y. Dorenkamp, S. M. Janke, M. Kammler, A. M. Wodtke and O. Bünermann, *Proc. Natl. Acad. Sci. U.S.A.*, 2018, **115**, 680–684.
365 S. Wille, H. Jiang, O. Bünermann, A. M. Wodtke, J. Behler and A. Kandratsenka, *Phys. Chem. Chem. Phys.*, 2020, **22**, 26113–26120.
366 P. Liang, E. V. F. De Aragão, G. Pannacci, G. Vanuzzo, A. Giustini, D. Marchione, P. Recio, F. Ferlin, D. Stranges, N. F. Lago, M. Rosi, P. Casavecchia and N. Balucani, *J. Phys. Chem. A*, 2023, **127**, 685–703.
367 S. Schauermann, N. Nilius, S. Shaikhutdinov and H.-J. Freund, *Acc. Chem. Res.*, 2013, **46**, 1673–1681.
368 S. Schauermann and H.-J. Freund, *Acc. Chem. Res.*, 2015, **48**, 2775–2782.
369 S. Attia, E. J. Spadafora, J. Hartmann, H.-J. Freund and S. Schauermann, *Rev. Sci. Instrum.*, 2019, **90**, 053903.
370 W. Ludwig, A. Savara, R. J. Madix, S. Schauermann and H.-J. Freund, *J. Phys. Chem. C*, 2012, **116**, 3539–3544.
371 A. Savara, W. Ludwig and S. Schauermann, *ChemPhysChem*, 2013, **14**, 1686–1695.
372 A. Savara, W. Ludwig, K.-H. Dostert and S. Schauermann, *J. Mol. Catal. A: Chem.*, 2013, **377**, 137–142.
373 C. Schroeder, A.-K. Baumann, M. C. Schmidt, J. Smyczek, P. A. Haugg, O.-C. Graap and S. Schauermann, *J. Phys. Chem. C*, 2022, **126**, 4907–4920.

374 K.-H. Dostert, C. P. O'Brien, F. Mirabella, F. Ivars-Barcelo, S. Attia, E. Spadafora, S. Schauermann and H.-J. Freund, *ACS Catal.*, 2017, **7**, 5523–5533.
375 K.-H. Dostert, C. P. O'Brien, F. Ivars-Barcelo, S. Schauermann and H.-J. Freund, *J. Am. Chem. Soc.*, 2015, **137**, 13496–13502.
376 J. Wulfes, A.-K. Baumann, T. Melchert, C. Schroeder and S. Schauermann, *Phys. Chem. Chem. Phys.*, 2022, **24**, 29480–29494.
377 J. Wulfes, A.-K. Baumann, M. Cieminski, C. Schroeder and S. Schauermann, *J. Catal.*, 2024, **429**, 115213.
378 C. D. Feldt, T. Kirschbaum, J. L. Low, W. Riedel and T. Risse, *Catal. Sci. Technol.*, 2022, **12**, 1418–1428.
379 C. D. Feldt, T. Gimm, R. Moreira, W. Riedel and T. Risse, *Phys. Chem. Chem. Phys.*, 2021, **23**, 21599–21605.
380 C. D. Feldt, P. A. Albrecht, S. Eltayeb, W. Riedel and T. Risse, *Chem. Commun.*, 2022, **58**, 4336–4339.
381 G. Wittstock, M. Baeumer, W. Dononelli, T. Kluener, L. Luehrs, C. Mahr, L. V. Moskaleva, M. Oezaslan, T. Risse, A. Rosenauer, A. Staubitz, J. Weissmueller and A. Wittstock, *Chem. Rev.*, 2023, **123**, 6716–6792.
382 B. Xu, R. J. Madix and C. M. Friend, *Acc. Chem. Res.*, 2014, **47**, 761–772.
383 B. J. Xu, X. Y. Liu, J. Haubrich, R. J. Madix and C. M. Friend, *Angew. Chem., Int. Ed.*, 2009, **48**, 4206–4209.
384 J. A. Schwarz and R. J. Madix, *Surf. Sci.*, 1974, **46**, 317–341.
385 M. P. D'Evelyn and R. J. Madix, *Surf. Sci. Rep.*, 1983, **3**, 413–495.
386 J. A. Fair and R. J. Madix, *J. Chem. Phys.*, 1980, **73**, 3486.
387 J. Neugebohren, D. Borodin, H. W. Hahn, J. Altschaffel, A. Kandratsenka, D. J. Auerbach, C. T. Campbell, D. Schwarzer, D. J. Harding, A. M. Wodtke and T. N. Kitsopoulos, *Nature*, 2018, **558**, 280.
388 D. Borodin, K. Golibrzuch, M. Schwarzer, J. Fingerhut, G. Skoulatakis, D. Schwarzer, T. Seelemann, T. Kitsopoulos and A. M. Wodtke, *ACS Catal.*, 2020, **10**, 14056–14066.
389 K. Papendorf, K. Golibrzuch, T. Zhong, S. Schwabe, T. N. Kitsopoulos and A. M. Wodtke, *Chem.: Methods*, 2022, **2**, e202200017.
390 K. Golibrzuch, P. R. Shirhatti, J. Geweke, J. Werdecker, A. Kandratsenka, D. J. Auerbach, A. M. Wodtke and C. Bartels, *J. Am. Chem. Soc.*, 2015, **137**, 1465–1475.
391 D. Borodin, M. Schwarzer, H. W. Hahn, J. Fingerhut, Y. Wang, D. J. Auerbach, H. Guo, J. Schroeder, T. N. Kitsopoulos and A. M. Wodtke, *Mol. Phys.*, 2021, **119**, e1966533.
392 J. Fingerhut, D. Borodin, L. Lecroart, M. Schwarzer, S. Hoerandl, A. Kandratsenka, D. J. Auerbach, A. M. Wodtke and T. N. Kitsopoulos, *J. Phys. Chem. A*, 2023, **127**, 142–152.
393 D. Borodin, I. Rahinov, O. Galparsoro, J. Fingerhut, M. Schwarzer, K. Golibrzuch, G. Skoulatakis, D. J. Auerbach, A. Kandratsenka, D. Schwarzer, T. N. Kitsopoulos and A. M. Wodtke, *J. Am. Chem. Soc.*, 2021, **143**, 18305–18316.
394 M. Schwarzer, N. Hertl, F. Nitz, D. Borodin, J. Fingerhut, T. N. Kitsopoulos and A. M. Wodtke, *J. Phys. Chem. C*, 2022, **126**, 14500–14508.

395 D. Borodin, N. Hertl, G. B. Park, M. Schwarzer, J. Fingerhut, Y. Wang, J. Zuo, F. Nitz, G. Skoulatakis, A. Kandratsenka, D. J. Auerbach, D. Schwarzer, H. Guo, T. N. Kitsopoulos and A. M. Wodtke, *Science*, 2022, **377**, 394–398.
396 D. Borodin, I. Rahinov, J. Fingerhut, M. Schwarzer, S. Hörandl, G. Skoulatakis, D. Schwarzer, T. N. Kitsopoulos and A. M. Wodtke, *J. Phys. Chem. C*, 2021, **125**, 11773–11781.
397 D. Borodin, O. Galparsoro, I. Rahinov, J. Fingerhut, M. Schwarzer, S. Horandl, D. J. Auerbach, A. Kandratsenka, D. Schwarzer, T. N. Kitsopoulos and A. M. Wodtke, *J. Am. Chem. Soc.*, 2022, **144**, 21791–21799.
398 C. T. Campbell, *Acc. Chem. Res.*, 2019, **52**, 984–993.
399 T. L. Silbaugh and C. T. Campbell, *J. Phys. Chem. C*, 2016, **120**, 25161–25172.
400 A. U. Nilekar, J. Greeley and M. Mavrikakis, *Angew. Chem., Int. Ed.*, 2006, **45**, 7046–7049.
401 L. Zhou, A. Kandratsenka, C. T. Campbell, A. Wodtke and H. Guo, *Angew. Chem., Int. Ed.*, 2019, **58**, 6916–6920.
402 J. Fingerhut, D. Borodin, M. Schwarzer, G. Skoulatakis, D. J. Auerbach, A. M. Wodtke and T. N. Kitsopoulos, *J. Phys. Chem. A*, 2021, **125**, 7396–7405.
403 T. L. Silbaugh, E. M. Karp and C. T. Campbell, *J. Am. Chem. Soc.*, 2014, **136**, 3964–3971.
404 D. J. Garton, A. L. Brunsvold, T. K. Minton, D. Troya, B. Maiti and G. C. Schatz, *J. Phys. Chem. A*, 2006, **110**, 1327–1341.
405 B. H. Wu, J. M. Zhang, T. K. Minton, K. G. McKendrick, J. M. Slattery, S. Yockel and G. C. Schatz, *J. Phys. Chem. C*, 2010, **114**, 4015–4027.
406 A. Caracciolo, J. C. S. Veliz, D. D. Lu, H. Guo, M. Meuwly and T. K. Minton, *J. Phys. Chem. A*, 2023, **127**, 8834–8848.
407 A. Caracciolo, J. M. Zhang, S. A. Lahankar and T. K. Minton, *J. Phys. Chem. A*, 2022, **126**, 2091–2102.
408 E. J. Smoll, M. A. Tesa-Serrate, S. M. Purcell, L. D'Andrea, D. W. Bruce, J. M. Slattery, M. L. Costen, T. K. Minton and K. G. McKendrick, *Faraday Discuss.*, 2018, **206**, 497–522.
409 S. M. Purcell, P. D. Lane, L. D'Andrea, N. S. Elstone, D. W. Bruce, J. M. Slattery, E. J. Smoll, S. J. Greaves, M. L. Costen, T. K. Minton and K. G. McKendrick, *J. Phys. Chem. B*, 2022, **126**, 1962–1979.
410 R. Nieman, M. Sands, Y. Q. Wang, T. K. Minton, E. E. Mussoni, J. Engerer and H. Guo, *Phys. Chem. Chem. Phys.*, 2023, **25**, 15479–15489.
411 J. S. Wright, A. Jones, B. Farmer, D. L. Rodman and T. K. Minton, *CEAS Space J.*, 2021, **13**, 399–413.
412 S. L. Lednovich and J. B. Fenn, *AICHE J.*, 1977, **23**, 454–459.
413 M. E. Saecker, S. T. Govoni, D. V. Kowalski, M. E. King and G. M. Nathanson, *Science*, 1991, **252**, 1421–1424.
414 G. M. Nathanson, *Annu. Rev. Phys. Chem.*, 2004, **55**, 231–255.
415 A. G. Knight, C. S. Olivares, M. J. Roman, D. R. Moon, P. D. Lane, M. L. Costen and K. G. McKendrick, *J. Chem. Phys.*, 2023, **158**, 244705.
416 D. J. Nesbitt, A. M. Zolot, J. R. Roscioli and M. Ryazanov, *Acc. Chem. Res.*, 2023, **56**, 700–711.
417 P. D. Lane, K. E. Moncrieff, S. J. Greaves, K. G. McKendrick and M. L. Costen, *J. Phys. Chem. C*, 2020, **124**, 16439–16448.
418 M. J. Roman, A. G. Knight, D. R. Moon, P. D. Lane, S. J. Greaves, M. L. Costen and K. G. McKendrick, *J. Chem. Phys.*, 2023, **158**, 244704.

419 P. D. Lane, T. Gstir, S. M. Purcell, M. Swierczewski, N. S. Elstone, D. W. Bruce, J. M. Slattery, M. L. Costen and K. G. McKendrick, *J. Phys. Chem. A*, 2023, **127**, 5580–5590.
420 M. A. Tesa-Serrate, E. J. Smoll Jr, L. D'Andrea, S. M. Purcell, M. L. Costen, D. W. Bruce, J. M. Slattery, T. K. Minton and K. G. McKendrick, *J. Phys. Chem. C*, 2016, **120**, 27369–27379.
421 W. A. Alexander, J. P. Wiens, T. K. Minton and G. M. Nathanson, *Science*, 2012, **335**, 1072–1075.
422 M. Faubel, S. Schlemmer and J. P. Toennies, *Z. Med. Phys.*, 1988, **10**, 269–277.
423 R. Dupuy, S. Thurmer, C. Richter, T. Buttersack, F. Trinter, B. Winter and H. Bluhm, *Acc. Chem. Res.*, 2023, **56**, 215–223.
424 B. Winter, S. Thürmer and I. Wilkinson, *Acc. Chem. Res.*, 2023, **56**, 77–85.
425 X. F. Gao, D. J. Hood, X. Y. Zhao and G. M. Nathanson, *J. Am. Chem. Soc.*, 2023, **145**, 10987–10990.
426 J. A. Faust, T. B. Sobyra and G. M. Nathanson, *J. Phys. Chem. Lett.*, 2016, **7**, 730–735.
427 T. B. Sobyra, H. Pliszka, T. H. Bertram and G. M. Nathanson, *J. Phys. Chem. A*, 2019, **123**, 8942–8953.
428 G. Taylor, *Proc. R. Soc. London, Ser. A*, 1960, **259**, 1–17.
429 D. K. Lancaster, A. M. Johnson, D. K. Burden, J. P. Wiens and G. M. Nathanson, *J. Phys. Chem. Lett.*, 2013, **4**, 3045–3049.
430 C. Lee, M. N. Pohl, I. A. Ramphal, W. Yang, B. Winter, B. Abel and D. M. Neumark, *J. Phys. Chem. A*, 2022, **126**, 3373–3383.
431 W. Yang, C. Lee, S. Saric, M. N. Pohl and D. M. Neumark, *J. Chem. Phys.*, 2023, **159**, 054704.
432 T. Buttersack, H. Haak, H. Bluhm, U. Hergenhahn, G. Meijer and B. Winter, *Struct. Dyn.*, 2023, **10**, 034901.
433 T. Takayanagi, N. Masaki, K. Nakamura, M. Okamoto, S. Sato and G. C. Schatz, *J. Chem. Phys.*, 1987, **86**, 6133–6139.
434 K. Reuter and M. Scheffler, *Phys. Rev. B: Condens. Matter Mater. Phys.*, 2006, **73**, 045433.
435 L.-P. Wang, A. Titov, R. McGibbon, F. Liu, V. S. Pande and T. J. Martinez, *Nat. Chem.*, 2014, **6**, 1044–1048.
436 C. A. Grambow, A. Jamal, Y.-P. Li, W. H. Green, J. Zador and Y. V. Suleimanov, *J. Am. Chem. Soc.*, 2018, **140**, 1035–1048.
437 R. van de Vijver and J. Zador, *Comput. Phys. Commun.*, 2020, **248**, 106947.
438 K. T. Schuett, M. Gastegger, A. Tkatchenko, K. R. Mueller and R. J. Maurer, *Nat. Commun.*, 2019, **10**, 5024.

